CZECH TECHNICAL UNIVERSITY IN PRAGUE

Faculty of Civil Engineering

Experimental Centre

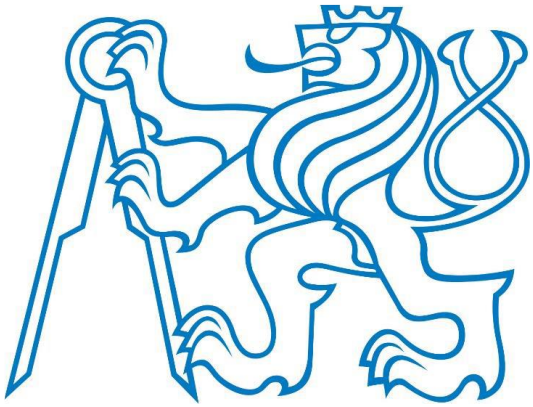

Diploma thesis

Biological Shielding Concrete and its Response to Elevated Temperatures

Vliv zvýšených teplot na chování betonu biologického stínění

2016/2017 Bc. Jaroslava Koťátková

Supervisor: Ing. Pavel Reiterman, Ph.D.

ČESKÉ VYSOKÉ UČENÍ TECHNICKÉ V PRAZE
Fakulta stavební
Thákurova 7, 166 29 Praha 6

ZADÁNÍ DIPLOMOVÉ PRÁCE

I. OSOBNÍ A STUDIJNÍ ÚDAJE

Příjmení: Koťátková Jméno: Jaroslava Osobní číslo: 396474

Zadávající katedra: K 210 - Experimentální centrum

Studijní program: Stavební inženýrství

Studijní obor: Materiálové inženýrství

II. ÚDAJE K DIPLOMOVÉ PRÁCI

Název diplomové práce: Vliv zvýšených teplot na beton biologického stínění

Název diplomové práce anglicky: Biological Shielding Concrete and Its Response to Elevated Temperatures

Pokyny pro vypracování:
Zpracování literární rešerše, která bude zaměřena na účinky vysokých teplot stíních betonů.
Příprava, realizace a vyhodnocení experimentálního programu se zaměřením na studium zvýšených teplot betonů různého složení. Závěrem práce bude diskuze dosažených experimentální výsledků v porovnání v dostupnou zahraniční literaturou.

Seznam doporučené literatury:
S. Alhajali, S. Yousef, B. Naoum, Appropriate concrete for nuclear reactor shielding, Applied Radiation and Isotopes 107 (2016) 29-32.
E.-S. A. Waly, M. A. Bourham, Comparative study of different concrete composition as gamma-ray shielding materials 85 (2015) 306-310.

Jméno vedoucího diplomové práce: Ing. Pavel Reiterman, Ph.D.

Datum zadání diplomové práce: 3.10.2016 Termín odevzdání diplomové práce: 6.1.2017

Podpis vedoucího práce | Podpis vedoucího katedry

III. PŘEVZETÍ ZADÁNÍ

Beru na vědomí, že jsem povinen vypracovat diplomovou práci samostatně, bez cizí pomoci, s výjimkou poskytnutých konzultací. Seznam použité literatury, jiných pramenů a jmen konzultantů je nutné uvést v diplomové práci a při citování postupovat v souladu s metodickou příručkou ČVUT „Jak psát vysokoškolské závěrečné práce" a metodickým pokynem ČVUT „O dodržování etických principů při přípravě vysokoškolských závěrečných prací".

Datum převzetí zadání | Podpis studenta(ky)

I hereby confirm that I have worked on my master´s thesis on my own, just with the methodical support of my supervisor Ing. Pavel Reiterman, Ph.D.

In addition, I declare all the references I have used to prepare this thesis are stated in the bibliography.

In Prague, 4th January 2017 …….

Bc. Jaroslava Koťátková

First and foremost, I would like to express my gratitude to my supervisor Ing. Pavel Reiterman, Ph.D. (Experimental centre, CTU) for his support, useful comments and remarks and for giving me the freedom to choose any topic possible. Furthermore, I would like to thank Ing. Jan Zatloukal, Ph.D. (Experimental centre, CTU) for many useful expert advice and language revisions. Also, I would like to thank Ing. Zbyněk Hlaváč, Ph.D. (CV Řež, s.r.o.) for introducing me to the topic and for inter-institutionary collaboration in the field. Last but not the least, I would like to thank LKAB Minerals for providing us with magnetite aggregate used in the experimental part of the thesis.

Abstract

The verification process of licenses for operation life of nuclear power plants (NPPs) is currently topical in many countries due to the high boom of NPPs´ construction in 1970s and 1980s, which means that the duration period of their original licences is close to the end. This process is highly controlled and requires detailed studies relating safety issues, which are verified by expert analyses and on-site testing. Therefore, the issue of understanding the degradation mechanisms of NPPs´ concrete structures, especially inside the containment, has become the interest of international agencies, national regulatory bodies as well as of many research institutions dealing with nuclear industry. Biological shielding concrete (BSC) serves the protection function of the surrounding environment, being the barrier which attenuates the majority of generated ionising radiation, and suffers from the negative effects of neutron and gamma irradiation accompanied by thermal loading. The effects of irradiation have not yet been researched in broad extent and the present bulk of information involves significant gaps. Moreover, the composition of BSC in many cases requires special design with the use of unconventional aggregate types. Although, the influence of heating on various types of concrete has been investigated widely, there is less data dealing with special concrete used as biological shield. Both areas therefore require further research, complemented with the development of tools determining the actual state of the NPPs´ concrete structures. This thesis is aimed at the investigation of thermal effects on five concrete types for use as BSC. Both destructive and non-destructive tests were conducted in order to investigate relationships between the concrete parameters, which can be easily obtained by NDT, and the actual degree of degradation, as the loss of mechanical properties achieved by destructive tests. The second main purpose was to give comparison of the performances between the studied concrete types differing only in the used aggregate.

Keywords: *biological shielding concrete, neutron radiation, gamma radiation, thermal loading, non-destructive testing, destructive testing, mechanical properties*

Abstrakt

Proces prodlužování platnosti licencí pro provoz jaderných elektráren (JE) je v současnosti aktuálním tématem v mnoha zemích, což vyplývá z mohutné výstavby JE v 70. a 80. letech minulého století, jejichž licencím nyní v blízké době vyprší platnost. Tento proces je přísně kontrolován a vyžaduje detailní studie týkající se otázek bezpečnosti podložené expertní analýzou a zkouškami in-situ. Z tohoto důvodu se porozumění degradačním mechanismům na konstrukcích JE, zvláště pak uvnitř kontejnmentu, stalo středem zájmu mezinárodních organizací, národních regulačních úřadů a mnoha výzkumných organizací v oblasti jaderného průmyslu. Beton biologického stínění (BBS) slouží jako bariéra chránící okolní prostředí od škodlivých účinků vznikajícího ionizujícího záření, přičemž je vystaven negativním vlivům neutronového záření a záření gama, doplněné tepelným zatížením. Dopady ozáření betonu na jeho vlastnosti nebyly dosud v příliš velkém rozsahu prostudovány a současný stav poznání obsahuje značné nedostatky. Kromě toho, složení BBS si v mnoha případech vyžaduje velmi specifický návrh převážně z hlediska použitého typu kameniva. Přestože vlivy vysokých teplot na degradaci mnoha druhů betonů jsou již poměrně dobře známy, informací o chování těchto specifických druhů betonů je podstatně méně. Z toho vyplývá, že obě zmíněné oblasti vyžadují pokračování ve výzkumných aktivitách společně s postupným vývojem nástrojů pro efektivní a průkazné určování reálného stavu betonových konstrukcí JE.

Tato diplomová práce je zaměřena na studium dopadu tepelného zatížení pěti vybraných reprezentativních druhů BBS s použitím jak destruktivních, tak nedestruktivních zkoušek, za účelem stanovení závislostí snadno získatelných parametrů prostřednictvím NDT na míře degradace, která je reprezentována poklesem hodnot mechanických vlastností získaných ze zkoušek destruktivních. Druhým důležitým účelem této práce bylo přímé porovnání chování jednotlivých druhů studovaných betonů, lišících se pouze druhem použitého kameniva, vystavených tepelnému zatěžování.

Klíčová slova: *beton biologického stínění, neutronové záření, gama záření, tepelné zatěžování, nedestruktivní testování, destruktivní testování, mechanické vlastnosti*

Table of contents

List of figures

List of tables

1 Introduction

In the member states of International Atomic Energy Agency (IAEA) there are currently more than four hundred nuclear reactors in operation and over sixty under construction, while the vast majority serves for commercial use in nuclear power plants (NPPs). The issue of NPPs operation raises disagreement in public and also amongst the authorities. In these days, the program of IAEA is on one hand increasingly supported in order to reduce the greenhouse gas emissions, on the other hand there is growing distrust in public regarding the safety assurance in nuclear industry, especially after the Fukushima Daiichi accident in 2011 [1]. The operation experience of NPPs has shown, that insufficient control of ageing process of its main structures can result in safety hazard and reduction of the plant service life [2].

Biological shields provide a protection barrier, preventing the escape of ionising radiation to the surrounding environment. Next to its use in NPPs, they find their vast significance also in nuclear medicine, which presents many indisputable benefits for the whole mankind. Therefore, the importance of understanding the deterioration mechanisms of biological shielding concrete structures is obvious.

1.1 Motivation

The operation time period of NPP structures are limited by the Atomic Energy Act, which grant licenses for certain duration, set in relation to economic and antitrust considerations (40 years in the United States and similarly in Europe varying case by case), although the service life of nuclear technologies is much longer. The regulatory bodies allow the renewal of licenses when safe operation is ensured. The prolongation of lifetime currently applies to a large number of NPPs as there was a boom in their construction in 1970s and 1980s [3]. Therefore, for safety assurance, the knowledge of degradation mechanisms of concrete structures in NPPs is of great importance.

The degradation of biological shielding concrete is induced by two major groups of deteriorating mechanisms. These are irradiation and related thermal loading. According to Fillmore [4] the temperature rise in concrete due to irradiation alone can reach 250°C. Such temperatures alone can cause severe damage to the concrete structure. There were many experiments and studies performed and the effects of high temperatures

on the behaviour of conventional concrete is well known [4-10]. However, in NPPs special concretes used for biological shielding are applied, whose properties under thermal loading are less researched. The effects of irradiation on the degradation degree are believed to be less significant, but the current knowledge of this problem is not sufficient. There are limited data partly because of the demandingness of experiments and partly due to the fact, that irradiation is always accompanied by the generation of heat, whose effects need to be excluded from the results evaluation. And thus, further research in both areas is necessary [10]. Next to this, the other essential issue is the ability to determine the degree of degradation by proper methods of non-destructive testing (NDT) in order to control the structural condition during its service life.

This diploma thesis will provide a comprehensive review of the adverse effects of gamma and neutron irradiation and thermal loading on biological shielding concrete. The investigation works regarding the irradiation effects on BSC exceeds the scope of this thesis and therefore, it will not be a part of the experimental programme. Five types of special concrete appropriate for biological shielding are investigated in the means of thermal loading effects. The loading temperatures and studied parameters are selected in relation to its use as a biological shield, preferentially in nuclear power plants. Both destructive and non-destructive testing are used in order to gain correlation of the measured non-destructive parameters with actual mechanical properties.

2 Biological shielding concrete

Any concrete, which serves as an inhibitory barrier against ionising radiation, may be identified as biological shielding concrete (BSC). Biological shields are necessary in nuclear industry as well as in medicine, research facilities and other particular industrial areas. In nuclear power plants, biological shielding walls surround the reactor pressure vessel (RPV) in order to provide the essential protection from radiation for the surrounding environment and experience the highest radiation exposure. In many NPPs, it also poses the function of load bearing structures supporting the RPV. Figure 1 shows the typical configuration of RPV and biological shielding structures in boiling water reactors (BWR) and pressurized water reactors (PWR), respectively. Next to its necessary function in NPPs, biological shields are needed practically in all applications, where the ionising radiation is somehow in high doses utilised. Such applications include radiology and radiotherapy in medicine, defectoscopy in industry, food-processing by radiation, hot cells in nuclear research facilities etc. Non-utilized source of ionising radiation is spent nuclear fuel from NPPs and other radioactive waste, which requires safe management with proper shielding barriers including BSC.

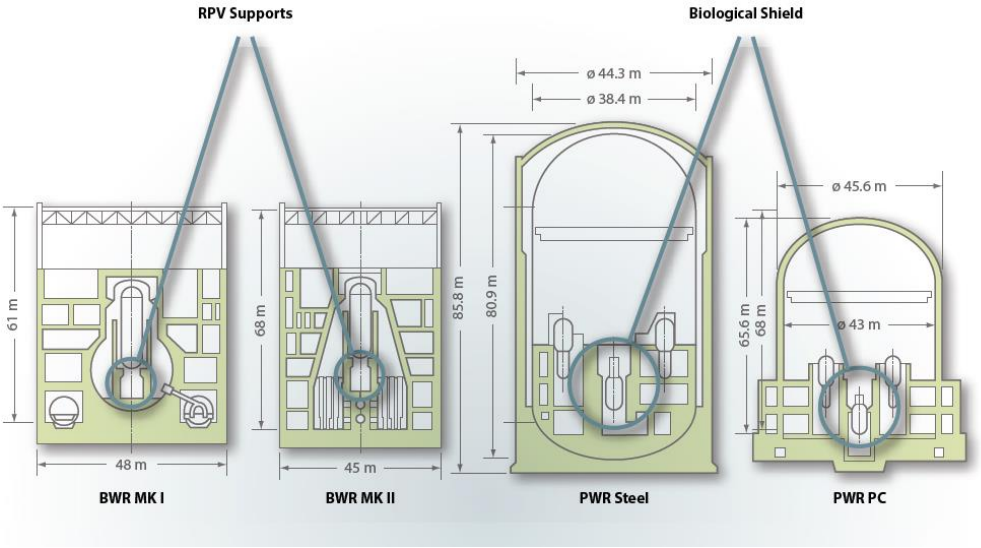

Figure 1: Vertical sections of boiling water reactor (BWR) and pressurized water reactor (PWR) containments with a designation of RPV and biological shield structures [11]

2.1 Radiation exposure

2.1.1 Types and sources of highly ionising radiation

The radiation, which quanta have energy high enough to ionise atoms or molecules, is referred to as ionising radiation. There are four types of ionising radiation: alfa, beta, gamma and neutron rays. When designing the mixture formulae of biological shielding concrete, it is necessary to consider the type, source and energy of the radiation, which is about to be shielded. Particularly dangerous penetrating radiation types are gamma or X-ray photons and neutron rays. Both gamma and X-rays are forms of electromagnetic radiation differing in wavelength and energy. While X-rays have wavelengths ranging from 0.01 to 10 nanometers and energies in the range 100 eV to 100 keV, gamma radiation is of lower wavelengths, less than 10 picometers (10^{-11} m), and corresponding higher energies - above 100 keV, which makes it a very penetrating radiation presenting serious hazards to human health. Conversely, neutron radiation is composed of free neutrons, which are emitted from a neutron source.

The **sources** producing some type of radiation, which need to be shielded, can be divided into three groups:

a) radioactive nuclides,
b) nuclear reactors,
c) particle accelerators.

Radioactive nuclides:

Radionuclides are in large number present in nature, but can be also produced artificially. These are nuclides with non-stable nuclei, i.e. with excess energy, which is released through the radioactive decay of the nuclide by emitting sub-atomic particles or gamma radiation. Gamma rays are of particular interest in the means of shielding needs, as they are of high energies and are used in several applications, such as in nuclear medicine and many other fields as mentioned above. Gamma radiation usually accompanies other forms of decay, such as alpha or beta, as the excited nuclear states are created in the decay of a parent radionuclide. There are many radioisotopes, which emit the highly energetic gamma photons during their radioactive decay, such as ^{60}Co, ^{137}Cs, ^{60}Ni, ^{241}Am, ^{192}Ir, ^{99}Tc etc. For example, cobalt-60, which is frequently used in radiotherapy, decays by beta decay to an exited state of ^{60}Ni, which further decays to its ground state emitting gamma photons of overall energy 2.5 MeV. An example of natural

source on Earth is potassium-40 with a very long half-life of 1.251×10^9 years, which is comparable to the age of Earth.

Even neutrons can be produced by a radionuclide source. There are three types of processes, which lead to neutron generation: (α, n) reactions, (γ, n) reactions or spontaneous fission. The mixing of a naturally occurring alpha emitter (e.g. radium) with a light element (e.g. beryllium) result in a reaction of an alpha particle with the nucleus of a light element emitting weakly bound neutrons. This reaction is known as a (α, n) reaction and is used in portable neutron sources. Also (γ, n) reactions are utilized as portable neutron sources, their advantage is the possibility of producing monoenergetic neutrons (unlike in case of (α, n) reactions) by simply removing the radioactive source (e.g. antimony-124) from the light element. Spontaneous fission (SF) neutron sources are produced by irradiating uranium or a transuranic element in a nuclear reactor, where neutrons are absorbed in the starting material and its subsequent reaction products, transmuting the starting material into the SF isotope. The most commonly used isotope is californium-252 [12,13].

Nuclear reactors:

The nucleus of a heavy atom can split into two nuclei (called fission products) when bombarded by particles (neutrons), releasing high amount of energy. In nuclear reactors, nuclei which release also other two or three neutrons during their split-up are used (uranium-235, uranium-233 and plutonium-239). This induces fission of further nuclei, which starts the **fission reaction chain** (see Figure 2). Uranium-235, which exists only as 0.7% of the naturally occurring uranium, undergoes nuclear fission with the release of ~ 180 MeV of energy per fission. There are two types of neutrons emitted during fission – prompt and delayed neutrons. Prompt neutrons are emitted within 10^{-8} seconds after fission and have energies of 4 – 14 MeV, which makes them the biggest concern in regard to shielding. Delayed neutrons have lower energies and present less than 1% of the overall emitted neutrons, therefore are not of major importance when concerning the shielding needs. Nuclear fission also results in the emission of gamma rays. Gamma photons emitted in a short time after fission (within 10^{-7} seconds) are referred to as "prompt" and produce high energies in the range of 0.3 – 10 MeV. Contrary, the "fission-product" gamma photons are emitted from a large number of un-stable isotopes, generated from the initial fission of the heavy element, during the following 20 minutes and present a

large contribution to the overall need-to-be-shielded radiation. Also, neutron inelastic scattering in about 10^{-14} seconds after the fission gives rise to gamma photons, which however need to be taken into account only in cases of neutron energies higher than 1 MeV. When designing the shielding concrete structures around the reactor pressure vessel, important factor is the production of "capture gamma photons" generated by (n, γ) reactions. When a nucleus of a specific matter absorbs a neutron, gamma capture photons are released, which happens in concrete shields. This secondary gamma radiation needs also to be shielded and is often the cause of large cross-section of concrete shields, as the neutron and gamma radiation have different requirements on the materials of BSC (see chapter 2.2). The interaction of neutrons with nuclei of a matter, which is exposed to neutron radiation, may cause the activation of the nuclei, leaving the matter radioactive for a long time. This makes the decommissioning of NPPs, after the nuclear reactor is shut down, very difficult. All these facilities need to be dealt as radioactive waste, as well as spent nuclear fuel. Rad-waste need to be disposed considering the safety issues, which once again calls for the urgent need of biological shields.

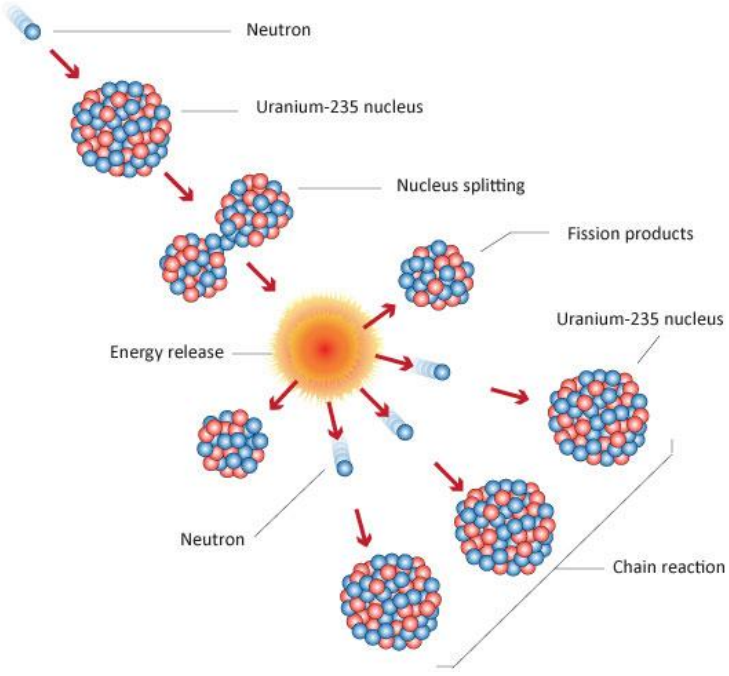

Figure 2: Fission chain reaction of Uranium-235 [13]

Another potential source of nuclear energy are **fusion systems**. Nuclear fusion is a reaction, in which two or more nuclei (e.g. deuterium and tritium) collide and thanks to its very high energy fuse together. Such a reaction is often accompanied by the emission

of energetic neutrons, which necessitate the provision of shielding. Next to the possible use of fusion in the next generation nuclear reactors, it can be also used for military purposes as thermonuclear weapons [12,13].

Particle accelerators:

When energetic electrons, which have been accelerated to high velocities, collide with a nucleus of heavy atoms, they are slowed down rapidly and emit intense electromagnetic radiation - a process called “Bremsstrahlung” or braking radiation. The emitted radiation in the form of X-ray photons can have energies from a few keV to several hundred MeV. X-ray generators are used in medicine for clinical therapy or diagnoses or in industry for non-destructive testing. Next to X-ray generators, other types of **electron accelerators** should be mentioned, such as van der Graaf accelerators, synchrotrons, betatrons, and cyclotrons. Moreover, when a fissile target is used, neutrons are produced via (n, γ) reactions. The Bremsstrahlung energy in the form of gamma radiation exceeds the binding energy of a neutron in the target. This phenomenon is used in neutron generators with the strength of 10^{13} neutrons/second.

In **ion-beam (or nucleon) accelerators**, kinetic energy is imparted to beams of ions, protons, deuterons or alpha particles of heavier nuclei with the use of electric and magnetic fields. Such energies are very high – in the range of GeV. Again, neutrons are produced when the accelerated particles strike nuclei of atoms, i.e. via (p, n), (d, n) and (α, n) reactions.

A short-lived plasma, which is produced by electromagnetic acceleration and compression in a **dense plasma focus (DPF),** cause nuclear fusion emitting X-ray radiation and neutrons. It can be used as neutron and X-ray source in medicine and industry [12,13].

2.1.2 Photon and neutron interaction with matter

As previously mentioned, the radiation types of interest in the means of shielding needs are photon rays (gamma radiation + X-ray) and neutron rays. Before discussing the materials used as BSC it is needed to understand the different mechanisms of radiation interactions with the matter of BSC.

Photon attenuation

Photons interact with shielding materials in three different ways, as photoelectric effect, Compton scattering, and pair production (see Figure 3). In photoelectric effect and pair production, gamma radiation is absorbed while ejecting an electron, in the latter case together with a positron. In the case of Compton scattering, the gamma rays are not absorbed but deflected via reduction of its energy, which was consumed during the ejection of an electron. This scattering process can be repeated several times in the BSC resulting in the rise of the actual amount of radiation passing through BSC.

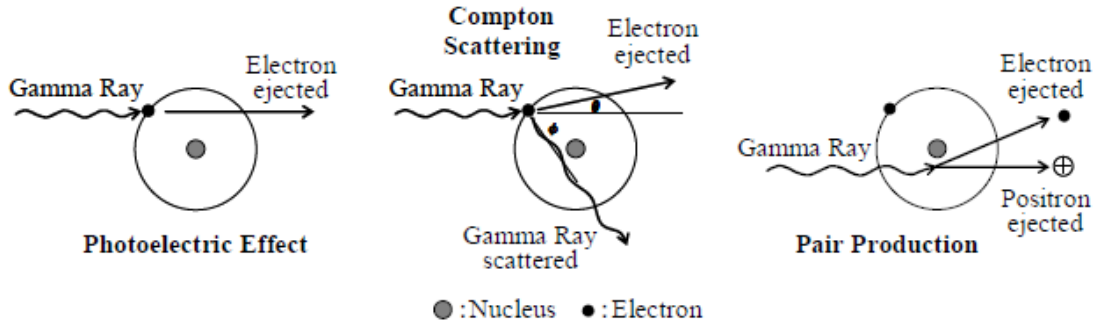

Figure 3: Three types of photon interactions with matter [14]

The prevailing type of interactions, which occur in the BSC, depend on the photon energy and the atomic number of the shielding material, which is shown in Figure 4. According to Kontani et al. [14], the energy range of gamma rays produced by nuclear reactors varies from 100 keV to 10 MeV. The dominant interaction mechanisms in this range for low atomic numbers is undesired Compton scattering.

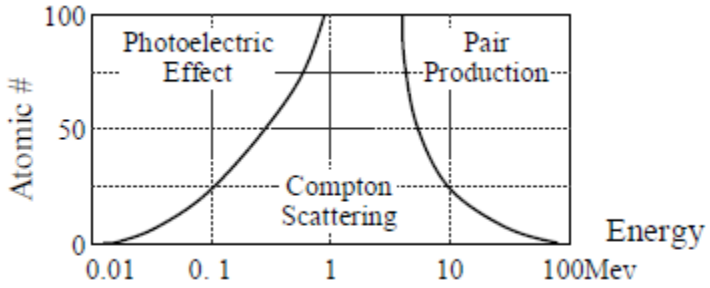

Figure 4: Relationship among gamma ray energy, atomic number, and interaction mechanisms [14]

As gamma radiation is attenuated by interactions with electrons, materials for shielding need to have high densities of these particles, therefore the use of materials with elements of higher atomic number is desirable. The high density of electrons in the

material can be ensured by using special cements, raising the compaction of concrete or using heavy aggregate. The easiest and the most often used way is the incorporation of high density aggregate.

Neutron attenuation

Neutrons interact with the atoms´ nuclei of the material. The mode of interaction depends mainly on the kinetic energy of the neutrons. According to its energy, neutrons can be classified into three groups:

a) thermal (so called slow) neutrons with energies less than 1 eV,
b) epithermal (so called intermediate or resonance) neutrons with energies between 1 eV – 0.1 MeV,
c) fast neutrons with energies above 0.1 MeV [15].

When talking about neutron absorption by a material, two terms should be clarified: *neutron fluence* and *neutron flux*. Neutron fluence is the number of neutrons *n* passing through a unit area – usually in units $n*cm^{-2}$. The overall dose of irradiation of concrete for a certain time period (e.g. for the operation life of a reactor) is usually expressed by the neutron fluence. Neutron flux is the rate of neutron radiation – typically in units $n*cm^{-2}s^{-1}$.

The collision of a neutron with matter can be of two types – inelastic and elastic scattering. The inelastic scattering occurs when the neutron is of high energy, i.e. a fast neutron. The fast neutron strikes a nucleus, changes direction and loses energy, which is consumed by the ejection of other neutron from the target nucleus and release of scattered gamma radiation. This process may be repeated many times until the fast neutron becomes an epithermal neutron. Elastic scattering is realized by collisions of epithermal neutrons, which do not have enough energy to force the nucleus to release gamma rays, however a neutron is ejected and the striking neutron loses some energy. This mechanism again repeats until the epithermal neutron becomes a thermal neutron. In the case of thermal neutron collision, all the energy is absorbed without releasing any type of particles.

The shielding concrete has to be designed taking into account all these factors. Firstly, the fast and intermediate neutrons have to be slowed down by inelastic and elastic scattering, where high density materials are needed to increase the number of atoms per

unit volume and thus the probability of the collision between neutrons and nuclei. Secondly, the decelerated neutrons, i.e. thermal neutrons, need to be absorbed or captured by the material in order to may be considered as removed from the incident neutron flux. For elastic scattering, materials containing **light elements** are necessary, as the epithermal and thermal neutrons can impart their energy only to much lighter nuclei according to the law of conservation of momentum. As the light element, hydrogen works very well and therefore **the presence of water** in the shielding material is of high importance.

Furthermore, the secondarily emitted gamma rays need to be taken into account on the top of the primary gamma radiation when calculating the shielding parameters of BSC.

2.2 Materials and design of BSC

Concrete is a very appropriate material for shielding purposes regarding nuclear power plants, particle accelerators, research reactors, hot cells, medical and industrial facilities, as it contains both heavy and light elements. Its composition can be designed according to the specific parameters of each application use.

2.2.1 Cement paste

As the main binding constituent for BSC various types of cement can be used. The most common is Ordinary Portland cement, but also special cements are sometimes chosen. There are five types of Portland cement available on market. The type of P-cement should be chosen considering the significant shrinkage and the generation of heat during the hydration of cement paste in large masses such as in case of BSC, which causes internal stresses. From this point of view, cements with pozzolanic additions are appropriate, e.g. Portland blast furnace slag cement, however many nuclear power plants are made of Ordinary Portland cement Type I, such as the Czech NPP Temelín [16].

Cement paste contains three forms of water, which is an essential source of hydrogen for neutron attenuation. These are free water, adsorbed (or physically bound) and chemically bound water. Free water is evaporated during cement hydration and, in the conditions of higher temperatures during irradiation, will be ultimately lost. When the temperatures increase, also the adsorbed water gradually escapes. The presence of

chemically bound water is therefore of higher importance and depends on the water/cement ratio, curing conditions, the age and mineral composition of the cement paste. The chemically bound water W_b can be approximately calculated, using the following relationship [17]:

$$W_b/C = a_1 (C_3S) + a_2 (C_2S) + a_3 (C_3A) + a_4 (C_4AF), \quad (1)$$

where C is the cement content, and C_3S, C_2S, C_3A, C_4AF, are the calculated fractional contents of the tricalcium silicate, dicalcium silicate, tricalcium aluminate and tetracalcium alumina-ferrite respectively with coefficients a_1 to a_4.

It has been reported, that the minimum amount of hydrogen in the cement paste should be 0.5% of the cement paste weight [18], which cannot be achieved using Ordinary Portland cement (OPC). Concrete with Portland cement paste usually contains hydrogen in about 0.25% by weight, which respond to about 23% of chemically bound water in the cement paste by weight [19,20]. In order to increase the chemically bound water amount in the cement paste, special types of cement can be used. However, as the cement paste present only about 15% of the concrete weight, it must be noted, that even though special kinds of cement may retain more water, the overall effect is not substantial. Therefore, the decisive factor would be the cement cost. An example of special cement appropriate for shielding concrete is barite cement, which is however not easily accessible and is expensive. A gypsum-alumina expansive cement was used in nuclear research reactors in the former USSR. The slightly increased water content (to about 25-30% by weight) does not overcome the undesired rapid loss of strength at temperatures of 160 – 200°C, which was later reported and thus is not anymore suitable for use [19]. Magnesium-oxychloride cement has three times higher water content in comparison to OPC, however for its corrosive action to steel is not appropriate for reinforced concrete structures. As the efforts to enhance concrete shielding properties by use of special cements were unsatisfactory, currently new ways are being searched, such as by modifying Portland cement concrete by a liquid polymer modifier or latex as a co-binder. The 10-20% of polymer in the binder serves as a source of hydrogen, participating in elastic scattering of neutrons [21,22].

2.2.2 Aggregate

As aggregate constitute at about 70-80% of concrete volume, it has a substantial effect on the concrete properties. For radiation shielding concrete, usually ordinary

normal-weight aggregate is used. However, it results in high cross-section of concrete structures to achieve satisfactory shielding parameters and thus, it is not rare to use heavy or other special aggregate according to the desired shielding characteristics at places, where there is not enough space for normal-weight concrete. Ordinary aggregate usually comes from local sources, typically consisting of calcareous or siliceous minerals with densities about 2 200 – 2 400 kg/m^3.

Special types of aggregate can be of natural origin or synthetic and can be divided into three groups:

a) heavy aggregate,
b) hydrous aggregate,
c) aggregate containing boron.

Heavy aggregate, or more precisely high-density aggregate, are generally used for shielding photons, i.e. gamma rays and X-rays. In addition, the high number of atoms per unit volume increases the total sum of inelastic neutron collisions, slowing down the fast neutrons. Hydrous aggregate contains bound water in its structure and thus are responsible for slowing down of intermediate neutrons and absorbing the thermal ones. As mentioned in chapter 2.1.2, the deceleration and absorption of neutrons is accompanied with the release of secondary high penetrating gamma radiation. For reduction of such effect, elements with large neutron cross-section, which are capable of emitting soft gamma rays that are readily absorbed by BSC, instead of elements releasing hard gamma radiation, are needed. The isotope boron-10 meets this requirement and thus boron or boron-compounds are often used in BSC for increased neutron capture.

Heavy aggregate

As heavy aggregate, minerals with bulk densities above 3000 kg/m^3 of both natural and synthetic origin are qualified. With its use, heavyweight concrete can be achieved, i.e. concrete of bulk densities higher than 2600 kg/m^3 according to ČSN EN 206-1 [23]. Iron ores, barite and ilmenite belong to the naturally occurring heavy aggregate, whilst as synthetic aggregate fillers ferrophosphorus, scrap iron or steel can be used. In Table 1 an overview of appropriate heavy aggregate, its bulk densities and the thickness of a BSC wall corresponding to 1 m thick ordinary concrete (OC) is listed.

Limonite and goethite belong to both groups of heavy and hydrous aggregate and will be discussed further on as well as *ferro-boron aggregate*, which is also of high density but due to the special effect of boron discussed in its own chapter.

Physical properties of *haematite* vary considerably between particular ores, some of them are soft, produce dust during handling and tend to be flaky, therefore could be problematic when used in concrete.

Ilmenite also show high varieties in physical properties amongst the particular ores and even within one deposit, as next to the crystalline ilmenite it usually further contains haematite, magnetite or other constituents. Ilmenite has been used as fine aggregate for shielding concrete in the USA, Australia and Canada, as it is a by-product from recovering of rutile, zirconium etc. from the ilmenite ores.

Magnetite is harder and more uniform than other iron ores, such as limonite or haematite, and its ores are the most used for BSC, as some formations are tough and coarse-grained with few impurities. As it is highly magnetic, special measures need to be taken, when used together with scrap steel/iron.

Barite concrete has been used mostly for research reactors, hot cells and so on in UK or USA. Its large sources and low cost explain its extensive use for structures in Oak Ridge National Laboratory, USA. Barite ores may contain minerals of opal or chalcedony, which are reactive when in contact with alkali and therefore it is recommended, that low purity barite ores should be used with low-alkali cements. Barite aggregate has rather weak structure and thus, should not be over-mixed. This is to avoid high abrasion producing soft particles, which could affect the cement-aggregate bond. Next to this, barite shows the highest thermal expansion, almost twice the value of other high-density aggregate. The second most common naturally occurring barium mineral is *witherite*, often found in veins of many rocks in association with barite or galena.

Ferrophosphorus, as a by-product from the manufacture of phosphorus, ranks among the group of synthetic aggregate. Ferrophosphorus has been reported to have low strength and abrasion resistance. At temperatures above 350 °C, the aggregate tends to oxidise in high rate with negative effects on the cement paste. Moreover, it can generate toxic inflammable gases, when used with Portland cement and thus must be used with caution [24].

Scrap iron or steel is produced as a waste from metals processing industry. The disadvantage is the difficulty in obtaining particles of suitable size and shape. The desired cubical or spherical shape of specific dimensions may be produced pointedly, but the cost considerably rises. Before use, it needs to be cleaned from oil and grease as early as possible to let a thin layer of rust to be formed, improving the bond with cement paste and reducing later corrosion, which could cause expansion, cracking and spalling of concrete. When combinations of the different types of aggregate are made, segregation is likely to occur and must be taken into account during the design of concrete composition.

Table 1: Overview of heavy aggregate appropriate for BSC [25]

	Chemical composition	**Bulk density [kg/m^3]**	**Thickness of BSC corresp. to 1 m OC [m/m]**
Limonite	$2Fe_2O_3 . 3H_2O$	3400 - 3800	0.75
Goethite	$Fe_2O_3 . H_2O$	3500 - 4500	-
Haematite	Fe_2O_3	4600 - 5200	-
Magnetite	Fe_3O_4	4600 - 5200	0.7
Barite	$BaSO_4$	4000 - 4400	0.7
Witherite	$BaCO_3$	aprrox. 4300	-
Ilmenite	$FeO . TiO_2$	4200 - 4800	-
Ferrophosphorus	$FeP / Fe_2P / Fe_3P$	5800 - 6300	0.48
Scrap-iron/steel	Fe	6500 - 7500	0.42
Ferro - boron	90% Fe, 10% B	approx. 5000	-

Hydrous aggregate

Hydrous aggregate contains chemically bound water, which is a constant source of shielding hydrogen nuclei, unlike the presence of free or physically bound water, which may completely evaporate especially at elevated temperatures. Some types of hydrous aggregate are also of high density and were listed above, such as limonite or goethite; other significant types are also serpentine and bauxite.

Serpentine aggregate *($3MgO.2SiO_2.2H_2O$)*, a source of previously widely used asbestos minerals (nowadays known as being harmful to human health), contain 10 - 12% of water by weight and is able to retain most of it up to 500 – 550°C. However, some serpentine rocks are weak and present low contents of hydrated water, which makes them unsuitable for radiation shielding concrete. Therefore, prior to the use of serpentine for BSC, the aggregate should be tested and meet certain specifications, which are for

example settled in American standard ASTM C637: Specification for Aggregates for Radiation-Shielding Concrete [26].

Bauxite ($Al_2O_3.2H_2O$) itself is a hydrated aluminium oxide, but bauxite ores generally contains many impurities, such as iron oxide or phosphorus. Bauxite is usually used for BSC only when the high cost excludes the use of other hydrous aggregate types.

Limonite is a hydrated iron oxide, which varies in quality and its water content can range from very low to 12% by weight, however it can be lost at temperatures of 200°C.

Goethite was reported to contain a bit less water than limonite, usually not exceeding 12%. Both limonite and goethite should be selected for BSC according to its water content, which is recommended being not less than 10% at temperature of 100°C. Some other types of hydrous aggregate can be also suitable for BSC, as for example in Oak Ridge National Laboratory calcined shale was used for shielding graphite reactor [12].

Boron-containing aggregate

The dose of *boron* in the aggregate has to be established carefully, because of the negative effects of boron on setting and hardening of fresh concrete. Recommended value according to ASTM C638 [27] is 1% by weight. Such prolonged setting can be counterbalanced by the use of proper accelerator. The boron can be incorporated in the form of borate minerals, synthetic boron frits, ground pyrex glass, boric acid, boron compounds dissolved in mixing water or as a cement constituent. Borate minerals, such as colemanite, borocalcite, ulexite, paigeite or tourmaline, originate from the precipitation of waters in arid volcanic regions. Borate deposits often contain impurities, such as clay, salts or gypsum, which negatively influence the concrete workability, setting time and strength.

Colemanite ($2CaO.3B_2O_3.5H_2O$) is the least soluble borate mineral found in nature and thus does not affect the concrete setting in such a large scale. The content of B_2O_3 in colemanite may vary from 15 to 51%. Low solubility was also recorded for *borocalcite ($CaO.2B_2O_3.4H_2O$)* with 40 - 50% content of B_2O_3. Lower solubility can be achieved by using synthetic boron substances, such as *boron frit glasses*. These are manufactured by melting boric acid or borax with calcium carbonate, silica and

eventually alumina. The decrease in solubility corresponds to the amount of Si and Al. Boron frits are of better quality compared to any natural boron minerals, but quite expensive and without any bound water. Even better properties were found for *boron carbides*, but their extremely high cost prevent their wider use for BSC. Other possible options could be the use of *ferroboron* or *colemanite-barite frits*.

2.2.3 Mixing and placing

The manufacture of BSC may be problematic, especially when incorporating heavyweight aggregate. The high differences between bulk density of cement paste and used types of aggregate is likely to result in segregation of fresh concrete. Achieving a good granulometry of heavyweight aggregate while considering cost and availability conditions is not an easy task. When using steel/iron scrap, it is beneficial to complement the steel/iron coarse aggregate with conventional sand or some type of natural high-density fine aggregate, e.g. soft limonite or ilmenite.

When placing is realized by standard methods and equipment, the batch size should be modified inversely proportional to the concrete density. Long chutes or pipes should be avoided and the layer thickness of the placed concrete should not exceed 300 mm. Formwork should be designed to withstand the extra load due to higher density of concrete [12,20].

Entrapped air minimization and sufficient compactness should be achieved through proper consolidation and/or using water-reducing additives. Vibration should be performed in two stages. Firstly, the frequencies higher than 50 kHz and amplitudes of about 1 mm should be applied to ensure good cohesiveness of concrete in order to fill the formwork without entrapping large voids of air on the formwork surface. Secondly, the frequencies of about 100 Hz and 200 - 230 Hz and amplitudes of 0.2 mm and 0.1 mm are the best choice to be applied for the activation of sand and cement paste respectively [20]. With higher amount of water-reducing agent and the consequent more flowable concrete, lower amplitudes and higher frequencies of vibration are needed. Heavyweight concrete requires shorter vibration intervals and special caution, as the aggregate is likely to settle expelling the cement paste resulting in bleeding. The bleed water should be removed while concrete is still plastic, otherwise it will result in delamination in the hardened concrete [20].

The pumping of high-density concrete is nowadays an accepted practice, however, it requires additional provisions on the top of the common demands on the properties of pumped concrete, such as higher pumping force. Pumping usually increase segregation and may cause pre-setting cracks at the interface with reinforcing bars and other obstacles. Therefore, higher attention should be paid to thickness of the concrete cover, which is crucial for durability properties of concrete and especially its reinforcement.

Lower risk of subsequent deterioration of concrete properties may be presented by alternative ways of placing, such as aggregate immersion or the grout intrusion, on the other hand, these requires either special facilities or in the latter case an expertise of the contractor [20].

2.3 Properties of biological shielding concrete

The function of biological shielding concrete can be manifold – the main purpose is to provide sufficient radiation shielding performance and the impingement shield in case of certain loss of coolant accident (LOCA) pipe breaks. These two are the only functions of BSC in case of a BWR reactor. But when considering biological shielding concrete in a PWR reactor, its static behaviour is also of high importance, as it provides a load-bearing support for the reactor pressure vessel (RPV). The BSC wall creates an internal structure inside the containment and serves as a load path to the foundations. Therefore, adequate values of mechanical properties are required, especially compressive and shear strength, as well as modulus of elasticity. In case of reactor types commercially used in the Czech Republic, VVER-440/213 and VVER-1000/320, the shielding structure is realized by a serpentine concrete annulus, which is sealed on all sides with steel plates and further supported by a concrete wall connected with the foundations. The shielding concrete thus in this case does not present the load-bearing function, but protects the load-bearing structures from irradiation by attenuating the majority of neutron and gamma rays. In such conditions, the shielding concrete may experience the rise in porosity or in extreme case local crumbling resulting in the rise of a cavity in the area of the highest stress, which could enable direct irradiation of the supporting concrete.

Next to this, due to the constant unilateral exposure of BSC to elevated temperatures, the thermal behaviour of BSC is essential. The thermal conductivity and

specific heat capacity are important characteristics from the point of view of stress distribution formed by the external heat source; and thermal expansion in the view of induced internal stress due to volume changes. High temperature gradient across the cross-section of the concrete block as well as aggregate swelling inside concrete may result in internal cracking and lead to deterioration.

Table 2 provides examples of biological shielding concrete properties containing different aggregate types that have been reported in literature in comparison to ordinary concrete [12]. It need to be noted, that the values have an indicative character, as the properties vary significantly from mix to mix depending on many factors, including composition design, manufacture, placing technique and curing conditions.

Table 2: Indicative values of biological shielding concrete properties reported in literature with comparison to ordinary concrete properties at 28 days age [12]

Property	Bulk density [kg/m^3]	Compressive strength [MPa]	Flexural strength [MPa]	Tensile strength [MPa]	Modulus of elasticity [GPa]	Thermal expansion [10^{-6} K^{-1}]	Thermal conductivity [W.m^{-1}.K^{-1}]	Specific heat [J.kg^{-1}.K^{-1}]	Drying shrinkage [%]
Barite	3 500 – 3 700	24.8 – 42.2	3.7	2.25 – 4.9	29.9 – 35.5	18	0.961 – 1.621	0.123 – 0.157	-
Serpentine	2 060 – 2 200	13.1-15.8	-	-		32	0.8	-	-
Limonite	2960	40.4	-	-	30.7	-	-	-	-
Haematite	3 730 – 4 200	16.2 – 89.6	-	-	37.3 – 69.1	-	-	-	-
Ferro-phosphorus	4 650	30.4	-	-	28.2	10.35	2.914	0.17	-
Magnetite	3 410 – 4 380	19.2 – 41.8	6.0	6.5	31.2 - 62	10.3	-	-	0.04
Limonite-iron	3 620 – 5 340	38.4 – 78.0	-	3.6-4.0	43.4 – 50.4	6.8 – 10.0	2.7 – 3.5	0.17 – 0.21	-
Pandermite-iron	5 330	27	1.6	1.6	29.6	-	3.5 (at 40°C)	753.624	0.026 (50%RH)
Iron shot	5 900	30 – 45	6.5	4.5	70	12.5	33	-	0.02
Ordinary concrete	2 300 – 2 400	30 - 40	5.5	3.5	20 - 30	8 - 15	1.9	-	0.04

3 Degradation of BSC - State of the art

The main factors inducing degradation of biological shielding concrete are the exposure to gamma rays, neutron radiation and thermal loading. Thermal loading is an accompanying effect of each of the latter two and cannot be avoided. In case of nuclear power plants, biological shield is exposed to all the types of deterioration and moreover in mutual enhancing effect. Ageing of concrete structures in NPPs is a highly acute problem, which is under interest of regulatory bodies, many researchers and NPP staff having responsibility for safety control. This chapter will provide a state-of-the-art of current knowledge relating all degradation mechanisms of BSC apart and its relationships as well as the consequences on the shielding properties of the material and the importance of water content.

3.1 Background

The current energy policy of IAEA member states varies considerably. Some states declared their will to divert from nuclear energy endeavouring to make use of renewable sources. Other states, who are aware of the insufficiency of these sources for their energy needs next to the problems with long-distance energy transfer and the difficulties in compensation of power fluctuations, are contrarily supporting the operation of nuclear power plants and extending their number, knowing that power generation from fossil fuels is no longer sustainable. As the majority of nuclear power plants are currently in stage of licences expiration, the operation prolongation approval needs to be gained. Although it is expected that the containment concrete structures are in very good state being able to meet their functional requirements, the process of licence granting requests a proven knowledge of the concrete performance. Several organizations have established research programs relating the ageing of concrete structures in NPPs and the tools for its monitoring, which include the U.S. Nuclear Regulatory Commission (U.S. NRC), the International Atomic Energy Association (IAEA), the American Concrete Institute (ACI), and the Electric Power Research Institute (EPRI) [4,10,28,29]. These programs are consisting of gathering the up to date knowledge of the degradation mechanisms, supporting relating research to fill its gaps and developing tools for monitoring, mainly through non-destructive testing.

The current state of understanding the aging process of BSC is based on research from the 1960s and 1970s studying the impact of elevated temperatures and heat on various types of concrete and the later investigations aimed mainly at the development of computational models of radiation damage [29-31]. The impact of elevated temperatures has been studied thoroughly on many types of concrete, however the comparison of the single concrete types in not easily managed as there is wide variety in the compositions, curing conditions, compaction and test configuration. The effects of irradiation have received significantly less attention and were in vast majority restricted to the computational modelling due to the difficulties in such a demanding process of samples irradiation and its consequent handling and testing. In these days the research is focusing on filling the knowledge gaps relating irradiation, while the effects of thermal loading are rather left aside, considered to be sufficiently understood. However, direct comparison of the various concrete types and the correlation of parameters gained from non-destructive testing and the actual degradation degree due to elevated temperatures have its meaning to complement the set of research data and make a coherent picture of the problem.

In 1978 Hilsdorf et al. [15] conducted a compilation study regarding the effects of irradiation on concrete structures. M.F. Kaplan in 1989 [12] published a wide review *Concrete of radiation shielding*, containing thorough explanations ranging from radiation physics to the degradation mechanisms of concrete. From that time, several NUREG reports were produced regarding both the thermal and irradiation effects on concrete structures in NPPs and many research articles were published. The later investigations disputed some findings of the Hilsdorf´s work and the most recent research works are aimed at filling the gaps in the knowledge of radiation-induced degradation.

3.2 Effects of thermal loading

Biological shielding concrete may be exposed to thermal loading from external sources as well as a result of internal heat evolution due to the capture of secondary gamma and neutron radiation. Temperatures, which can be reached within the concrete shield, are according to Fillmore [4] up to 250°C, which is enough to induce changes in microstructure and porous system of concrete and thus adversely affect its mechanical properties. The new-generation reactor concepts are of primary interest, as the concrete can be exposed to long-term steady-state temperatures in excess of 65°C, which is the

limit value of heat generation inside concrete by the present *American Society of Mechanical Engineers Pressure Vessel and Piping Code (ASME Code)* [32]. The influence of elevated temperatures on concrete has been investigated in wide extent [3-9,33], but there are many specifications, which makes it a complex problem, such as the encapsulation of water vapour and thermal gradients inducing additional stresses, thermal cycling, long duration of thermal loading, specific mix composition of concrete for nuclear applications and others. Therefore, the comparison of experiments is often difficult, as the conditions vary and in some cases are not mentioned in the study.

3.2.1 Temperature rise in biological shielding concrete

Due to the relatively low thermal conductivity of concrete the removal of the generated heat on the inner side or, thanks to gamma and neutron radiation capture, inside concrete is difficult. As a consequence, temperature fields inside concrete are non-uniform, which gives rise to differential thermal stresses [34]. From this point of view, it is needed to assess a correlation between the maximum incident energy flux and the tolerable compressive and tensile stresses to avoid cracking leading to local damage of the concrete structure [20]. It was reported, that reinforced concrete showed no damage when exposed to 268 $J.s^{-1}m^{-2}$, which within a 1.37 metre thick concrete block induced a temperature rise of 52°C. On the other hand, a concrete block of the same geometry and composition but without reinforcement exhibited surface cracking at a heat flux of only 33 $J.s^{-1}m^{-2}$ which caused temperature rise of 8.9°C. When temperature of 65°C was reached, internal compressive stresses in the concrete of the order of 7 MPa were produced [35].

In order to minimize the rise of internal thermal stresses, the concrete composition needs to be designed to gain these desirable properties: high thermal conductivity to minimise the heat build up, low coefficient of thermal expansion to minimise strains due to temperature gradients, and low drying shrinkage to minimise differential strains. It is possible to take into account creep and shrinkage, which may in certain cases reduce the internal stresses, computational models have been reported for example in studies of A. Samarin [36], D. McDonald et al. [37] and Y. Le Pape [38].

3.2.2 Summary of general behaviour of BSC

The effect of elevated temperatures can be evaluated on macroscopic and microscopic levels. The macroscopic damage includes additional stresses due to thermal

gradients in the concrete shield induced by irradiation. According to Abdo and Amin [39] the depression in the heat generation reaches about 60% at 40 and 10 cm in the R- and Z-directions, respectively. Induced thermal stresses depend on the coefficient of thermal expansion, modulus of elasticity, and Poisson's ratio. These properties are being changed with time due to both irradiation and heat and depend on the material compositions.

The second scale level is microscopic, which presents the changes in the cement paste, aggregate and transition zone between these two phases. The cement paste key factors determining its behaviour under elevated temperatures are: moisture state, chemical structure (bound water within C-S-H phase, CaO/SiO_2 ratio, amount of $Ca(OH)_2$) and physical structure (pore system and amorphous/crystalline phase ratio) [40]. Most aggregate types are stable at low temperatures - structural changes of siliceous aggregate appear at 573°C, opal specifically shrinks at 373°C, but other types can withstand higher temperatures. However, the interactions between cement paste and aggregate are of importance even at lower temperatures. At 20 – 80°C the loss of free water takes place, up to 150°C water permeability significantly increases and the dehydration of ettringite occurs, followed by the loss of physically bound water and the start of decomposition of the strength-bearing phase C-S-H gel at about 200°C [33]. Cement paste due to the evaporation of free and bound water shows a marked shrinkage while aggregate due to the increasing temperature expands [4,12,33]. The highest value of stresses induced by microscopic thermal changes are at the interface of the cement paste and aggregate which is the place of first cracking. There is a linear increase of thermal expansion of concrete up to 200°C and above this level a rapid rise due to the changes in the crystal structure of the aggregate and the failure of the transition bond. Siliceous aggregate shows greater expansion than calcareous. A wide review summarizing the effects of high temperatures on the properties of concrete was published by Kaplan [12]. Wide differences in physical and mechanical properties of concrete when exposed to elevated temperatures were reported due to not only the variations in mix composition and nature of used materials, but also due to different conditions of the carried tests. According to Pihlajavaara [12,41] up to eighteen parameters are needed to be considered when comparing results. These factors are rarely described in full detail, which results in data variations, sometimes even in contradictions.

The important issue relating the thermally loaded concrete is its **volume changes**. As indicated above, cement paste under lightly elevated temperatures mostly shrinks due

to the escape of free water followed by physically bound water. On the other hand, most types of aggregate experience swelling when exposed to heat. Shrinkage of cement paste causes the growth of small cracks, which weakens the bond between aggregate and the paste. The coincident expansion of the filler particles induces high stresses inside the concrete microstructure and lead to the deterioration of the material mechanical properties. A linear increase of thermal expansion up to 200°C and subsequent rapid rise due to the changes in the crystal structure of the aggregate and the failure of the transition bond has been reported [4,33]. However, the damage degree depends mostly on the type of used aggregate. For example, siliceous aggregate behaves much worse in comparison to other kinds, reaching almost two times higher expansion at 600°C than the calcareous ones. The compressive strength of concrete is also affected by the relative humidity, as the strength decreases from high RH to 40-50 % RH and increases with further decrease of RH. Drying of cement paste forms large pores, which are responsible for lowering of the concrete strength at high RH, but also tightens the layered structure of C-S-H, which it a phenomenon that prevails at low RH and result in the increase of strength.

The volume changes and the destruction of bond between single phases generally (for all concrete types) cause reduction in **compressive strength** up to 90°C, which is followed by strength recovering up to 200°C. The strength gain is caused by additional hydration of non-hydrated cement particles thanks to its interaction with escaping water. Above 200°C the chemical and mineralogical changes take place resulting in irreversible loss of strength. Figure 5 presents a summary of thermal loading effects on different concrete types. There are factors of testing conditions, which significantly influence the values of obtained results. These are the state in which the specimens are tested, i.e. hot or after cooling, the rate of cooling and whether the sample is unsealed or sealed during testing, as in the case of containment structures of Czech power plants, which is realized by steel plates. Sealed concrete shows lower strength compared to unsealed specimen thanks to the entrapment of water vapour causing an internal pore pressure rise [3,8]. Relating the cooling regime, Lee et al. [8] stated that cooling generates significant damage in unsealed concrete. On the other hand, for sealed specimens the results vary and no clear conclusion can be made [3,8]. Tensile strength appears to be affected in higher extent than compressive strength, but the available data is rare [3]. Experiments determining changes in modulus of elasticity due to heating showed wide variations in results, but generally above 100°C residual ratio was even less than in case of

compressive and tensile strength [12]. In nuclear power plants concrete structures are, due to the cessations of reactor operation for fuel exchange or others, exposed to the cycling of thermal load, which may induce material fatigue. More pronounced reduction in strength is often recorded during the first cycles and its higher effect was found to be on sealed samples [3].

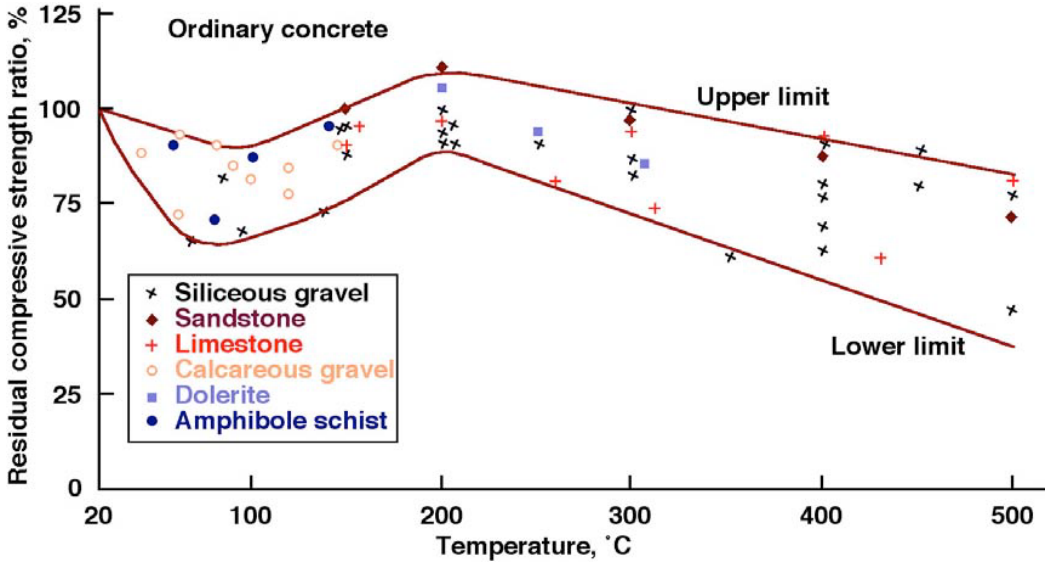

Figure 5: Effects of elevated temperatures on compressive strength of concrete differing in aggregate type [12]

3.2.3 Behaviour of BSC types reported in literature

The behaviour of certain types of biological shielding concrete under elevated temperatures has been studied and reported in literature. A short review of the data from available literature will be introduced.

Serpentine Concrete

Ohgishi et al. [42] investigated the properties of a serpentinite (a metamorphosed rock with serpentine as the primer mineral) concrete with density of 2 085 kg/m^3 and 28-day compressive strength of 19.3 MPa. Together with, also an ophicalcite concrete was studied, as ophicalcite is a type of marble containing serpentine spots. Water-cured and afterwards dried specimen were exposed to for 30 minutes to temperatures of 100°C, 200°C and 600°C. Samples of ophicalcite concrete were tested both hot and after being cooled to room temperature, while serpeninite samples just after heating. The decrease in density of serpentinite concrete was also monitored. Results are presented in Figure 6. Specimens tested hot correspond to the summary graph reported by Kaplan (Figure 5, chapter 3.2.2). It can be seen, that samples tested after cooling show higher degree of

damage with rising temperature, which is the result of additional damage processes during cooling, such as cracking induced by temperature gradients.

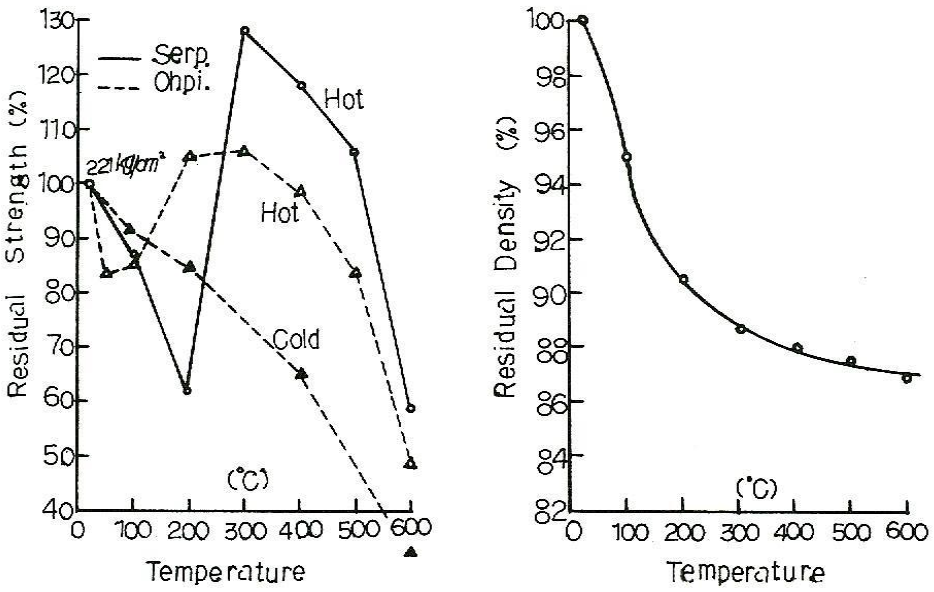

Figure 6: Serpeninite and ophicalcite concrete behaviour under elevated temperatures – effects on compressive strength of both concrete types - samples tested hot and of ophicalcite tested cold (left); and effects on density of serpentinite concrete (right) [42]

Serpentine-iron and serpentine-magnetite concrete were studied in conjunction with the N-Production Reactor located at Hanford, Washington [43]. Serpentine-iron concrete was placed by a preplaced aggregate method, while serpentine-magnetite by conventional placement, where serpentine presented about 46% of the total aggregate weight. Values of mechanical and physical properties obtained subsequently at rising temperatures are presented in the overall Table 3. The values of compressive strength also agree with the Figure 5 (chapter 3.2.2), as the residual ratio decreased at 85°C and further increased up to 200°C.

Ferrophosphorus concrete

Also ferrophosphorus concrete was part of the investigations carried on the N-Production Reactor at Hanford [43]. Concrete of density 4 650 kg/m^3 was produced from 19-mm maximum size ferrophosphorus aggregate, Type II Portland cement as the binder component and water/cement ratio 0.53 were set. Obtained results are also summarized in the overall Table 3. Ferrophosphorus concrete showed lower variations in the obtained values compared to serpentine-iron concrete.

Limonite concrete

Concrete containing limonite aggregate was studied by Desov et al. [44] and showed residual strength of 94, 88 and 85% at 100, 150 and 200°C respectively compared to the reference strength at room temperature. Davis et al. [45] reported data from the experiment of thermal loading of concrete containing mixture of aggregate – limonite, haematite and magnetite, referred as hydrous-iron concrete. Type II Portland cement was used with 0.43 water/cement ratio. After 28 days the specimens were heated and left to cool down before testing. Table 3 provides the summary of the obtained data.

Table 3: Overview of values of the properties of serpentine-iron, serpentine-magnetite, ferrophosphorus and hydrous-iron (mixture of limonite, haematite and magnetite) concrete exposed to elevated temperatures

	Type of aggregate	Density [kg/m^3]	Coefficient of thermal expansion [10^{-6} K^{-1}]	Compressive strength [MPa]	Modulus of rupture [MPa]	Static modulus of elasticity [GPa]	Dynamic modulus of elasticity [GPa]	Bond strength [MPa]	Length change [%]
Value at 90 days									
at 90 days	**Serpentine-iron**	3 530	8.66	31.2	3.4	27.5	37.2	6.2	+0.011
	Magnetite-serp.	3 050	-	36.1	5.3	34.2	39.0	3.2	+0.007
	Ferrophosporus	4 700	10.2	56.8	6.2	28.2	-	8.3	-0.053
	Hydrous-iron	3 590	9.93	73.7	6.4	57.8	-	8.1	-0.006
Residual ratio [%]									
85°C	**Serpentine-iron**	96	109	53	48	-	44	-	-0.036
	Magnetite-serp.	95	-	109	110	85	80	67	-0.041
	Ferrophosporus	98	108	99	125	-	-	-	-0.123
	Hydrous-iron	99	96	69	109	-	-	-	-0.020
140°C	**Serpentine-iron**	-	-	92	-	-	-	-	-
	Magnetite-serp.	94	-	113	97	65	63	61	-0.065
	Ferrophosporus	-	-	-	-	-	-	-	-
	Hydrous-iron	-	-	-	-	-	-	-	-
200°C	**Serpentine-iron**	96	119	139	29	60	42	17	-0.049
	Magnetite-serp.	94	-	116	90	57	54	28	-0.073
	Ferrophosporus	98	118	96	94	65	-	50	-0.140
	Hydrous-iron	97	91	64	100	70	-	86	-0.058
350°C	**Serpentine-iron**	95	127	122	11	44	27	3	-0.021
	Magnetite-serp.	95	-	98	61	43	35	11	-0.149
	Ferrophosporus	97	114	80	75	45	-	47	-
	Hydrous-iron	94	83	65	90	48	-	34	-0.111

Magnetite concrete

Magnetite concrete samples were also tested by Ohgishi et al [42]. Results of the experiment performed on cylindrical samples in comparison to ordinary concrete are presented in

Figure 7. The magnetite concrete showed slightly better resistance to elevated temperatures compared to ordinary concrete. It may be the result of higher thermal conductivity of magnetite and thus the better transfer of heat balancing the thermal gradients.

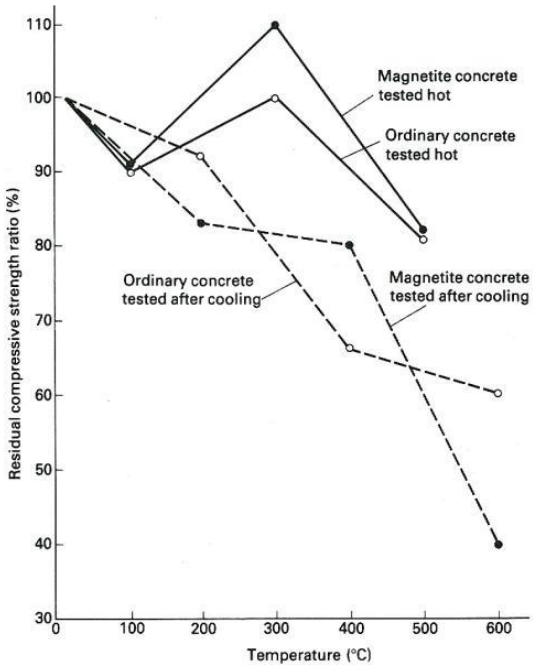

Figure 7: Residual compressive strength of magnetite and ordinary concrete exposed to elevated temperatures [42]

An investigation of magnetite concrete used in French reactor EL4 [46] showed the rise in mechanical properties of samples when stored for 120 days at 110°C (after the curing period of 150 days in 20°C) compared to samples stored on air for the whole time period – see Table 4. Even after thermal cycling the values of mechanical properties did not show any significant decrease. The concrete was made of Portland cement with water/cement ratio of 0.63 and at standard laboratory conditions (after 28-days of air-storage at 50% relative humidity) had density 3550 kg/m^3 and compressive strength 28.3 MPa.

Table 4: Effect of elevated temperatures of the properties of magnetite concrete used in Reactor EL4 in France

	Cured in water at 20°C			Cured in air at 50% RH and 20°C		
	Compressive strength [MPa]	Flexural strength [MPa]	Dynamic modulus of elasticity [GPa]	Compressive strength [MPa]	Flexural strength [MPa]	Dynamic modulus of elasticity [GPa]
270 days at 20°C	41.0	4.2	58.3	35.0	3.1	44.2
150 days at 20°C followed by 120 days at 110°C	53.0	4.2	52.0	42.0	3.8	40.5
150 days at 20°C followed three thermal cycles from 20 to 110°C	52.0	3.0	-	35.0	2.75	-

Haematite concrete

Haematite concrete (with the use of Portland cement) showed very similar behaviour as magnetite concrete when exposed to elevated temperatures, as firstly a decrease of strength was recorded at 100 and 150°C followed by high increase at 300°C, reaching 150% residual compressive strength ratio. However, when alumina cement was used the ratios were 80, 35 and 55% [47], which was surprising as alumina cement is known to have much better resistance to elevated temperatures compared to Portland cement.

Several investigations with different binder composition have been carried out, during the development of concrete design for use as biological shield of a liquid-sodium cooled fast reactor in Italy [48]. Pozzolanic cement as well as a proprietary binder mixture, containing Portland cement, plasticizer, expansive cement, and anti-bleeding agent, were used. Both concretes showed superior behaviour when exposed to heating up to 300°C, showing residual strength ratios of 91 – 145% compared to non-heated samples. For all studied mixes, the residual strength was higher for samples tested after cooling than samples tested hot, contrary to the above mentioned investigations on magnetite or ophicalcite concrete.

Barite concrete

Barite aggregate concrete has been investigated under the EUROATOM Programme as a possible shielding material for nuclear reactors [49] and was compared to ordinary concrete with limestone aggregate. Results showed superior behaviour of the barite concrete, which was attributed to the better compatibility of the barite aggregate with the cement matrix compared to limestone.

Weigler and Fisher [50] studied the effects of elevated temperatures on concrete containing barite and quartz aggregate and incorporating either Portland or Blast-furnace cement, with water/cement ratio 0.6 in both cases, which is presented in Figure 8. Barite concrete performed better in the means of compressive strength decrease, weight loss and the resistance to the load of 1/3 of the ultimate strength under the elevated temperatures, as it showed no strength loss. Also, thermal cycling to 600°C resulted in no additional strength loss, which was certainly not the case of quartz. In this case, the compressive strength of hot samples was lower than for samples tested after cooling.

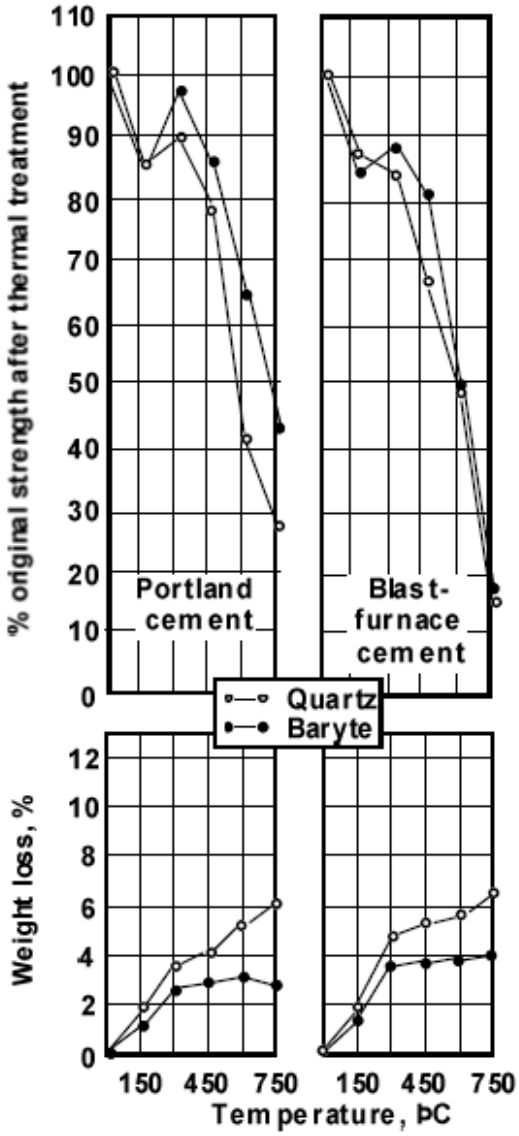

Figure 8: Weight loss and residual compressive strength after thermal treatment of barite and quartz aggregate concrete [50]

Sakr and Hakim [51] also reported the better behaviour of barite concrete compared to normal weight gravel concrete under elevated temperatures. Next to this, the decrease of shielding properties was investigated. The radiation attenuation coefficient for a Cobalt-60 source decreased by 9.5, 13.0, 17.0, and 21.0% after the exposition for 2 hours at 250˚, 500˚, 750˚, and 950˚C, respectively; similar results were obtained for Caesium-127 source. The decrease in the shielding ability was the result of the deterioration of concrete physical and mechanical properties, mainly the density drop, which was induced by the loss of different forms of water.

A long-term experiment was conducted at the Saclay Nuclear Centre in France [52], where the barite concrete samples were exposed to heating at 150 and 250°C for 28, 90 and 180 days. The data from the experiment can be seen in Table 5. The residual ratios are significantly low when considering that temperatures of 100°C on the BSC surface are not so rare and even temperatures of 250°C has been reported to be recorded, although probably not continuously in such a long term.

Table 5: Mechanical properties of a barite concrete exposed to elevated temperatures for periods of 28, 90 and 180 days

Concrete property	**Residual ratio [%]**					
	150°C			250°C		
	28 days	90 days	180 days	28 days	90 days	180 days
Compressive strength [MPa]	112	93	72	97	80	62
Compressive strength [MPa]	96	81	76	60	54	53
Static modulus of elasticity [GPa]	62	38	38	42	30	27

Ilmenite concrete

Ilmenite concrete was a part of the Sakr and Hakim´s study [51], which revealed its better performance under elevated temperatures compared to barite and normal-weight gravel concrete, as well as higher attenuation coefficient. A comparison of obtained values is made in Table 6. All studied mixes used Portland cement, water/cement ratio was set as 0.40 and maximum aggregate size as 20 mm, in case of barite and ilmenite concrete sufficient dose of plasticizer was needed. The study also showed higher values of all studied properties for sealed samples compared to unsealed ones for normal-weight gravel concrete.

Table 6: Comparison of properties of barite, ilmenite and normal-weight gravel concrete and compressive strength residual ratio under elevated temperatures [51]

Concrete type/property		Barite concrete	Ilmenite concrete	Gravel concrete
28-day values	Density [kg/m^3]	3 250	3 450	2 350
	Compressive strength [MPa]	47	51	44
	Tensile strength [MPa]	2.85	3.53	2.55
	Flexural strength [MPa]	4.42	5.4	3.43
	Modulus of elasticity [GPa]	29.03	34.43	20.79
	Attenuation coefficient for Cobalt-60 source (1330 keV)	15.97	16.59	12.72
Residual ratio of compressive strength [%]	250°C	93.5	93.3	83.6
	500°C	60.1	84.7	41.4
	750°C	31.9	58.7	15.0
	950°C	14.4	26.3	0.0
Residual ratio of attenuation coefficient for Cobalt-60 source (1330 keV) [%]	250°C	90.5	88.1	90.6
	500°C	87.0	86.0	86.6
	750°C	83.0	84.0	84.0
	950°C	79.0	22.0	75.1

Iron (steel) shot concrete

Davis et al. [53] studied effects of elevated temperatures on the properties of Portland cement mortars with steel shots and recorded firstly decreasing and later on, at temperatures above 350°C, slightly increasing density. This was in correlation of initial contraction of samples at temperatures up to 350°C followed by expansion at 600°C. The increases in both density and length was attributed to the higher rate of oxidation of iron shots at high temperatures, however temperatures above 600°C are not common for concrete of biological shield.

Portland cement concrete containing iron/steel shot as aggregate was studied by Arshinov [47], who recorded rising compressive strength in the temperatures range 100 - 200°C, as the reported residual ratios at 100, 150, 200 and 300°C were 83, 113, 133 and 133% respectively. On the other hand, a decrease in strength at 200°C was reported by Desov [44], however the water/cement ratio was much higher (0.75) compared to Arshinov´s concrete (0.40).

3.3 Effects of irradiation

The irradiation effects on the physical and mechanical properties of BSC have been investigated in lesser extent and need further study [10]. The prolongation of NNPs operation life-time has invoked the revival of research, with particular interest in the expected radiation exposure (fluence or dose) of concrete structures inside the containment [54] .

The current state of understanding of radiation effects on concrete structures is based only on data from test reactors. The accelerated conditions however do not simulate the real conditions inside the containment precisely and so far, it is not clear if the rate-effects of accelerated irradiation correspond to the higher damage of long-term exposure for a given dose [55]. Such knowledge gaps are nowadays under focus of researchers in states, which are currently dealing with prolongation of their NPPs operation, and are included in the research of plant life management programs.

In Japan, after the Fukushima Daiichi accident, new nuclear regulations were adopted together with an approval system for extending operating periods of NPPs. The Japanese run a national project organized by Japan Nuclear Energy Safety Organization aiming at the effects of concrete irradiation, as Hilsdorf´s review was found to be insufficient, lacking data regarding the concrete types used for light water reactors (LWR) [56]. The energy program of United States relies on nuclear power to meet future national energy needs while reducing the greenhouse gas emissions. The Electric Power Research Institute and Oak Ridge National Laboratory established a research plan to investigate the aging and degradation processes of NPPs concrete structures [57]. In Spain, the decommissioned Jose Cabrera nuclear power station or so called “Zorita NPP” serves as a source of concrete samples, which underwent irradiation during the Zorita´s operating life. In January 2010, Spanish Strategic Platform on Nuclear Research and Development established a working group on Zorita´s concrete cores to research the effects of high radiation and temperatures on concrete.

Due to the need of understanding the degradation processes of NPP concrete, which is topical all around the world, research organizations and utilities have agreed upon establishing the International Committee on Irradiated Concrete (ICIC). The purposes of ICIC are to provide a forum of timely information exchange among the member organizations, promote broad application of specialized or unique investigation

techniques, facilitate conception, planning and guidance of new research programs and promotes cross-institutional use of resources [57].

3.3.1 Up-to-date knowledge

An extensive review was conducted by Hilsdorf et al. [15], who gathered the so far available data into diagrams of fluence/dose vs. residual strength ratio and stated a neutron fluence of 1.0×10^{19} n/cm^2 as an outline for the display of the detrimental effects. This work was afterwards questioned by some authors [58,59], as many of the experiment conditions were not proper or were not edited and thus the data may not be relevant. The suggested threshold levels of neutron and gamma fluences vary among different authors and authorities and has not yet been agreed upon. The ACI committee [28], conforming to Hilsdorf´s work, stated the value of 1.0×10^{21} n/cm^2 as the level of loss of mechanical properties and placed a conservative limit of 1.0×10^{13} n/cm^2, while British Standards Institute [60] stated 5.0×10^{17} n/cm^2 for neutron fluence as a safe limit. Maruyama et al. [58] proposed levels for fast neutrons of 1.0×10^{20} n/cm^2 and for gamma irradiation of 2.0×10^{10} rad (2.0×10^{8} Gy). Modified Hilsdorf´s diagrams by Maruyama et al. [58] are presented in Figure 9.

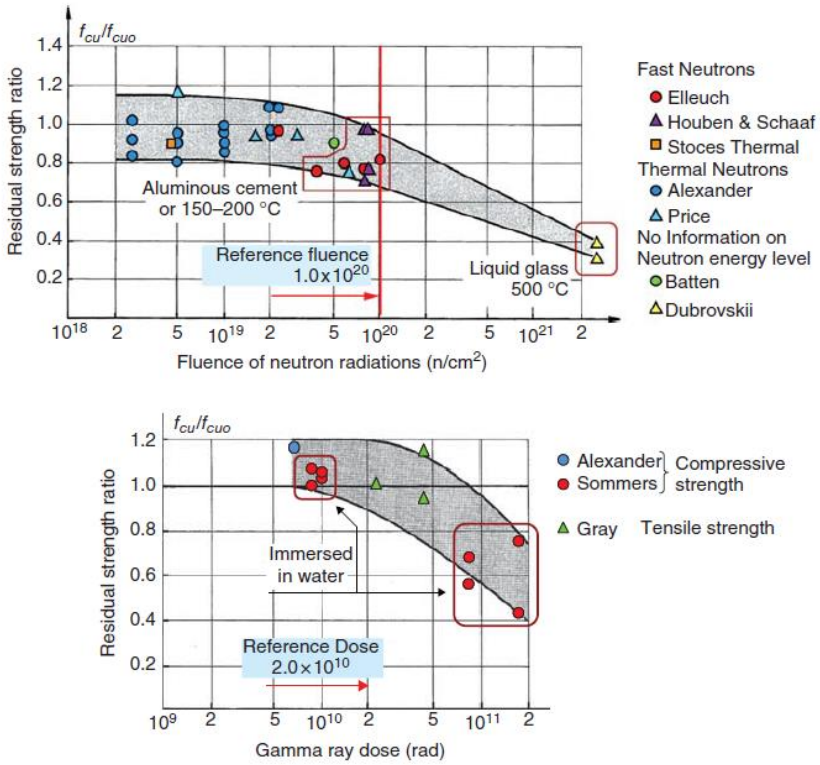

Figure 9: Modified Hilsdorf´s diagrams of fluence/dose vs. residual strength ratio [59]

Unfortunately, most of the published studies up to now did not consider the prolonged service of NPPs lifetime above 40 years and thus increased exposure of concrete structures to radiation. Only few researchers conducted experiments to higher fluences than 1.0×10^{19} n/cm^2 [61-66] and in most studies there is not sufficient information on neutron energy, type of the used aggregate and other details of the experiments, many investigations also did not separate the effects of higher temperatures. K.G. Field et al. [67] updated the reviews of Hilsdorf [15] and Kontani [59,68] with the supplement of new data focusing mainly on neutron irradiation, which will be presented in section 3.3.3.

3.3.2 Effects of gamma irradiation

According to Kontani´s work [59,68] gamma and neutron irradiation effects should be evaluated separately on hydrated (or water) phases and crystalline (or solid) phases. Gamma rays have adverse effects predominantly on the hydrated phases, i.e. cement paste, whilst rather crystalline aggregate stays almost unaffected. Moreover, Kontani found out, that gamma rays have very little effect on compressive strength of concrete and as well, the majority of other studies was focused on the neutron irradiation rather than on the effects of gamma rays. Gamma rays from reactors contain energy from 100 keV to 10 MeV and because of the rather low atomic numbers of elements present in cement paste and aggregates, gamma rays primarily decay by Compton scattering (see Figure 4, chapter 2.1.2). Compton scattering is a process of gamma ray collision with an orbital electron inducing the ejection of an electron, and thus reducing the energy of the gamma ray and changing its travelling direction, which means that the gamma ray is not directly absorbed and it may further interact with the material. The interaction of gamma rays with the single phases of concrete are listed in Regarding the solid phases, gamma rays have negative impact mainly on materials with anisotropic chemical bonds, such as covalent bonds, while ionic and metallic bonds stay unaffected. Therefore, siliceous materials degrade by gamma irradiation to higher degree, compared to other constituents, through breaking of Si-O bonds. On the other hand, since the energies of ejected electrons due to Compton scattering are very low, they do not have significant impact on the solid phases of cement paste and aggregate [14].

Next important issue is the interaction of gamma rays with water in the cement paste, which results in the evaporation of water vapour or in the excitation of the water molecules. The imparted energy then causes the decomposition of the exited molecule

with the release of gaseous hydrogen and oxygen or/and the hydrogen peroxide, eventually other radicals, which can react with the cement paste. The decrease of water amount through water radiolysis or evaporation can be caused due to the direct effect of gamma rays or by the generated heat accompanying gamma irradiation. On the other hand, the heating may result in additional hydration of unreacted cement particles, which may slightly increase the strength of concrete.

Table 7. Regarding the solid phases, gamma rays have negative impact mainly on materials with anisotropic chemical bonds, such as covalent bonds, while ionic and metallic bonds stay unaffected. Therefore, siliceous materials degrade by gamma irradiation to higher degree, compared to other constituents, through breaking of Si-O bonds. On the other hand, since the energies of ejected electrons due to Compton scattering are very low, they do not have significant impact on the solid phases of cement paste and aggregate [14].

Next important issue is the interaction of gamma rays with water in the cement paste, which results in the evaporation of water vapour or in the excitation of the water molecules. The imparted energy then causes the decomposition of the exited molecule with the release of gaseous hydrogen and oxygen or/and the hydrogen peroxide, eventually other radicals, which can react with the cement paste. The decrease of water amount through water radiolysis or evaporation can be caused due to the direct effect of gamma rays or by the generated heat accompanying gamma irradiation. On the other hand, the heating may result in additional hydration of unreacted cement particles, which may slightly increase the strength of concrete.

Table 7: The interaction of gamma rays with cement paste and aggregate [14]

	Water phase	**Solid phase**	
Cement paste	• Water may be decomposed by radiolysis to generate hydrogen and hydrogen peroxide, which in turn decomposes into water and oxygen. • Gamma heating may cause additional hydration of unhydrated cement and transformation to hydrated cement. • Hydrogen peroxide generated in radiolysis process may react with cement paste.	• SiO bond of calcium silicate hydrate in cement paste may be slightly decomposed due to the covalent nature of the bond.	• Electrons are ejected by scattering of gamma rays and collide with the solid phases of cement paste or aggregates.
Aggregate	• Small amount of water may be released by the radiolysis in the form of hydrogen and oxygen gases as well as by gamma heating in the form of vapour.	• Siliceous aggregate may be slightly decomposed.	

The role of peroxide, released by water radiolysis due to gamma irradiation, was studied by Bouoniol and Aspart [69]. The peroxide in aqueous solution with the presence of calcium and water easily form a metastable calcium peroxide octahydrate:

$$Ca(OH)_{2\,aq} + H_2O_2 + 6H_2O \rightarrow CaO_2.8H_2O \downarrow \quad (1)$$

Which further decomposes, leading to a **carbonation process of concrete**:

$$CaO_2.8H_2O \rightarrow CaO_2 + 8H_2O \quad (2)$$

$$CaO_2 + H_2O \rightarrow Ca(OH)_2 + \frac{1}{2} O_2 \quad (3)$$

$$Ca(OH)_2 + CO_2 \rightarrow CaCO_3 + H_2O \quad (4)$$

The carbonation products, i.e. calcite, fills the pores of concrete leading to the decrease in porosity. But similarly, as in case of carbonation of concrete on air, the pH of concrete reduces as a result of the consumption of $Ca(OH)_2$ leading to the corrosion of the concrete reinforcement (if reinforced). Moreover, if an excessive amount of calcite if formed, it may lead to formation of microcracks, eventually resulting in the reduction of strength. The negative aspect of irradiation-induced carbonation is the fact that it occurs throughout the whole volume of the concrete structure as it is not dependant on the presence of CO_2 from air and thus it is not restricted to the surface layer. This was approved by the study of Vodák et al. [70]. Figure 10 shows the decrease in porosity after gamma irradiation of concrete samples, the disappearance of the peak in the pore size distributions around 10 to 20 nm is visible.

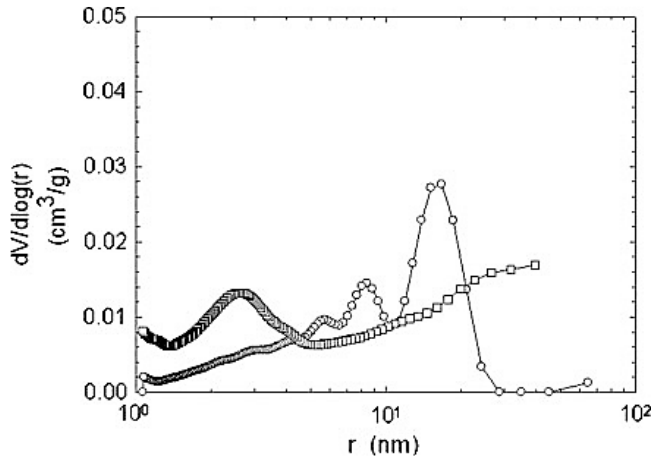

Figure 10: The pore size distributions of irradiated (1 MGy) and unirradiated concrete specimens in the centre of concrete sample. Open circles are unirradiated samples. Open squares are irradiated samples [70].

The gamma irradiation tests can be easily performed on its own with the use of gamma sources, contrary to neutron irradiation, which is always accompanied by emitting gamma rays. Gamma radiation results in water release as well as the effects of thermal loading and thus, in order to assess the amount of released water due to gamma rays, the irradiation tests must be performed along with thermal loading experiments. When the amount of water released by thermal loading is known (which can be assessed by TG/DTA analyses – see Figure 11), the released water due to gamma irradiation can be quantified, as in the experiment of Kontani et al. at the Takasaki Advanced Radiation Research Institute of Japan Atomic Energy Agency [71], where cobalt-60 was used as the source of gamma radiation. The water released due to gamma irradiation can be of two forms: water vapour because of gamma ray heating and water decomposition with the formation of free hydrogen and oxygen (radiolysis) as it was recorded in the Kontani´s experiment, the results are presented in Figure 12. The evaporation of water vapour takes about 40 - 50 days from the start of the irradiation process, contrary to the gaseous hydrogen release which lasts about 100 days, however the percentage of water radiolysis is very small. Moreover, an important finding was made in the experiment – the water radiolysis occurred only in case of the free water or physically bound water leaving the chemically bound water intact, which would mean that the hydration products were unaffected as well [71].

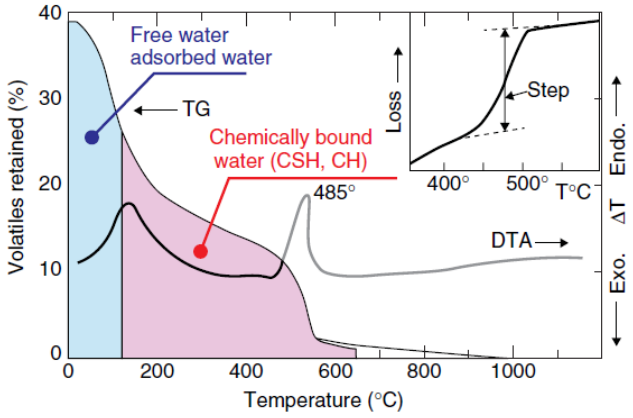

Figure 11: Volatiles retained versus temperature (TG/DTA) [71]

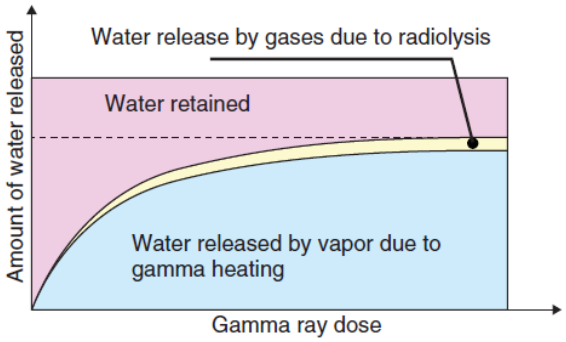

Figure 12: Amount of water released vs. gamma ray dose [71]

The **compressive strength** of concrete exposed to gamma radiation has not been widely investigated and a threshold value was set as 2.0×10^8 Gy (2.0×10^{10} rad) by Kontani et al. [71] and Electric Power Research Institute proposed a slightly more conservative value of 1.0×10^8 Gy (1.0×10^{10} rad) [10]. However, studies of Vodák et al. [72] and Soo and Milian [73] showed that the decrease in concrete strength may occur at significantly lower doses of gamma irradiation depending on the dose rate, e.g. at 1.0×10^5 Gy (at Co-60 gamma flux of 31 Gy/hr). However, at higher dose rate the decrease in strength occurred at 10^7 Gy. The explanation for this phenomenon has not been reported.

Data relating the changes in tensile strength and modulus of elasticity under gamma irradiation is very limited and there is wide scatter in results, therefore no direct conclusions can be derived. Further very important factor is **creep**, as it in certain degree controls the mechanical response of concrete structures under load. Creep on one hand negatively affects the pre-stressed concrete as it responsible for relaxing the pre-stress in rebars, but on the other hand it may mitigate the crack propagation [57]. According to the study of McDowall [74], the concrete creep reduced, while autogeneous shrinkage increased under gamma irradiation. Whittmann [75] recorded the same behaviour of concrete in experiments performed at low relative humidity, which indicates that the water radiolysis may be the forcing factor. However, these properties, i.e. creep and shrinkage, as well as tensile strength and modulus of elasticity, require further research in order to make relevant conclusions.

3.3.3 Effects of neutron irradiation

As neutrons interact with matter by collisions with the atoms´ nuclei it is likely, that the lattice structure is modified, which may be manifested through the change of

physical and mechanical properties of the material. Well crystalized and dense materials are therefore more prone to be adversely affected by neutrons rather than amorphous materials with high porosity. So in concrete, as mentioned above, the aggregate as a well crystalized material is the vulnerable phase in relation to neutron irradiation. The cement paste experience some degree of damage, but due to its high porosity and randomly layered internal structure the alternation of its physical and mechanical properties is very low [10]. Table 8 provides an overview of neutron interactions with concrete phases.

Table 8: The interaction of neutrons with cement paste and aggregate [14]

	Water phase	**Solid phase**
Cement paste	Molecular products from water may be the same as those for gamma rays, but the yields are different due to the different LET*	Although dislocation of atoms in solid cement particles may take place, the lattice defect by the distortion may not be accumulated, and the deformation of the paste may be negligible due to the porosity of the paste and the fineness of the cement particles
Aggregate	Interaction with water is the same as that in cement paste	Lattice constants are increased due to the dislocation of atoms, and lattice effects are accumulated

*LET = Linear Energy Transfer, which is the amount of radiation energy deposited in matter per unit particle path length in Joules per meter or keV/μm

Irradiation of concrete leads to the metamorphism of aggregate. The former crystalline grains undergo the transition into a certain degree of amorphization, which induces partial conversion of the former anisotropic concrete to its isotropic state. This is accompanied with changes in several properties, such as optical, physical and mainly mechanical characteristics. The important factor is the volumetric changes of aggregate, as its expansion initiate cracks in the concrete microstructure, especially in the case of aggregate with covalent bonds (e.g. quartz) [57]. The conversion of aggregate may be also in some cases attached with the precipitation of oxides or the formation of cavities.

The incomplete and inaccurate Hilsdorf´s compilation of data with the modifications by other authors was once again reviewed and updated by K.G. Field [67]. The updated data are summarized in Figures 13 – 16. It was concluded that a marked decrease of relative **compressive strength** occurs at fluences above $1.0 – 2.0 \times 10^{19}$ n/cm^2 reaching 50% of the earlier proposed value of 1.0×10^{20} n/cm^2 by Maruyama et al. [58] for the worst cases (Figure 13). It was noted that the compressive strength of cement paste can be reduced by induced thermal loading and gamma rays or by interactions with the aggregate changes (differential thermal expansion or swelling) due to neutron irradiation. However, the dominant factor in the concrete strength changes

is the intrinsic properties of the aggregate, which was demonstrated by works of Seeberger [76], Hilsdorf [15], Gray [77] and Kelly et al. [78]. The **tensile strength** is more pronouncedly affected by neutron irradiation than compressive strength. This can be of great importance, as tensile strength is directly associated with shear load capacity. Residual tensile strength at values near 2.0×10^{19} n/cm^2 were in the worst cases only at 25% of the initial value, while the effect of higher temperatures due to irradiation is not very significant. This indicates that the neutron irradiation itself may have an essential detrimental effects on the shear behaviour of concrete. On the other hand, there is higher scatter in results than in the case of compressive strength revealing the higher sensitivity of tensile strength to the concrete composition [67,79] and also the available data is less in number (Figure 14). Even less studies were conducted with respect to **modulus of elasticity** and the majority of them were performed at temperatures above 100°C. From such limited data, a threshold level for marked decrease in modulus of elasticity was found to be 2.0×10^{19} n/cm^2 of neutron fluence (Figure 15). According to Schneider et. al. [80] the decrease depends strongly on the type of aggregate, as lower residual ratios were found for siliceous concrete compared to other types.

The weight loss during irradiation is mostly caused by the accompanying elevated temperatures inducing the escape of free water. According to authors who observed weight loss due to irradiation and simultaneously due to exposition to thermal loading in accordance with irradiation temperatures [81,82] showed no or very little differences.

Contrary, the **changes in volume** are of high importance. A significant matter of interest should be the radiation induced volumetric expansion (**RIVE**) as the expansions are notably greater than the ones related to ASR or thermal loading and it is believed to be the major factor responsible for the deterioration of mechanical properties of concrete [83]. Swelling is observed for concrete exposed to fluences above 1.0×10^{18} n/cm^2 with enhanced effects above 1.0×10^{19} n/cm^2 (Figure 16). The worst behaviour was found for concrete with siliceous aggregate compared to carbonate and heavy weight aggregate [33,77,78]. The expansion at a fluence of 5×10^{19} n/cm^2 is about 1% for limestone and flint, and about 0.1% for serpentine. This can be attributed to its susceptibility for low fluence amorphization and related swelling, next to the high thermal expansion coefficients. Moreover, in biological shielding concrete (BSC) surrounding the reactor pressure vessel, the radiation field's strong attenuation produces a high RIVE gradient [38]. This causes high biaxial compressive elastic stresses in the vertical and

hoop directions near the reactor cavity and important elastic tensile hoop stresses toward the back of the BSC [77]. This together with temperature and moisture content gradients affects the mechanical properties of concrete. In particular, it leads to the development of lower strengths toward the reactor cavity [64].

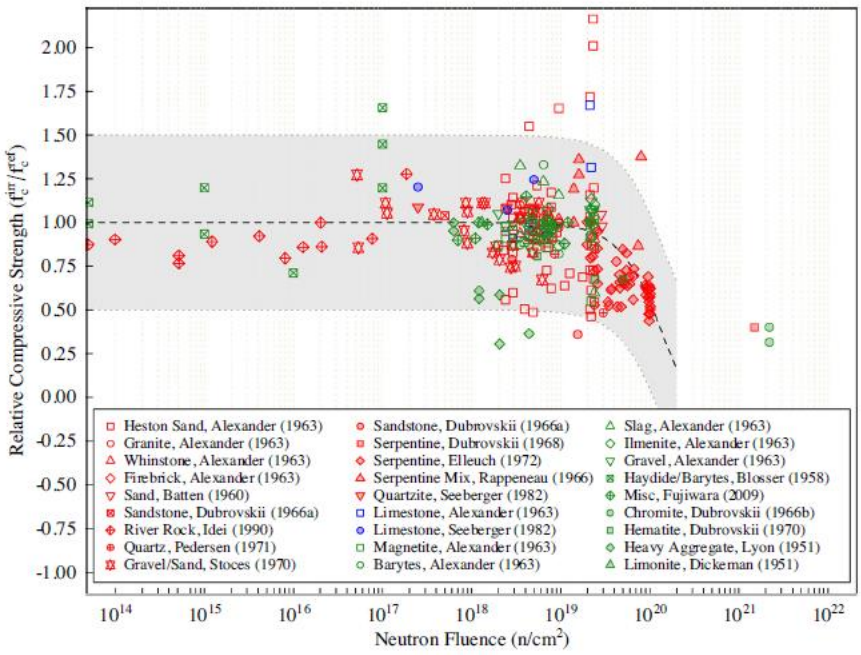

Figure 13: Relative compressive strength of concrete and mortar specimens versus neutron fluence [67]

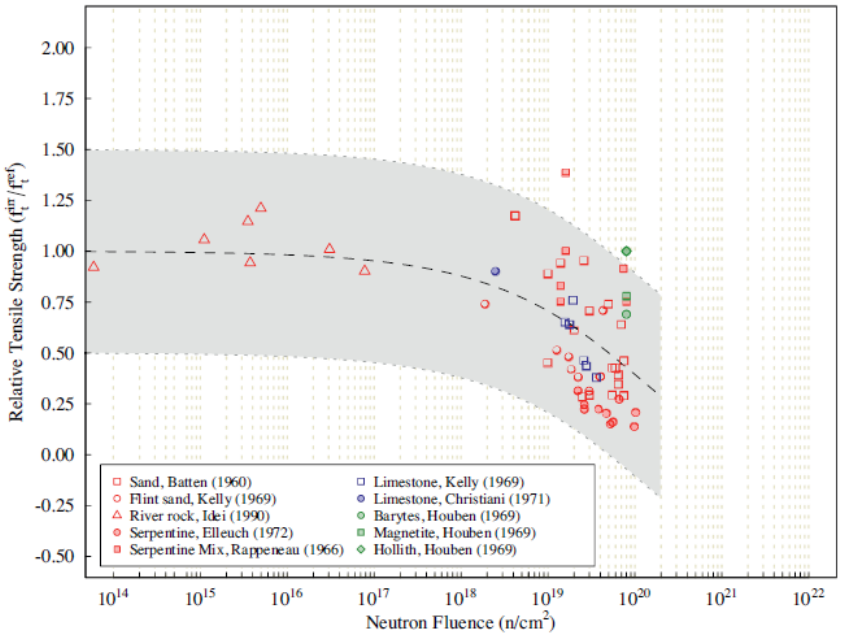

Figure 14: Relative tensile strength of concrete and mortar specimens versus neutron fluence [67]

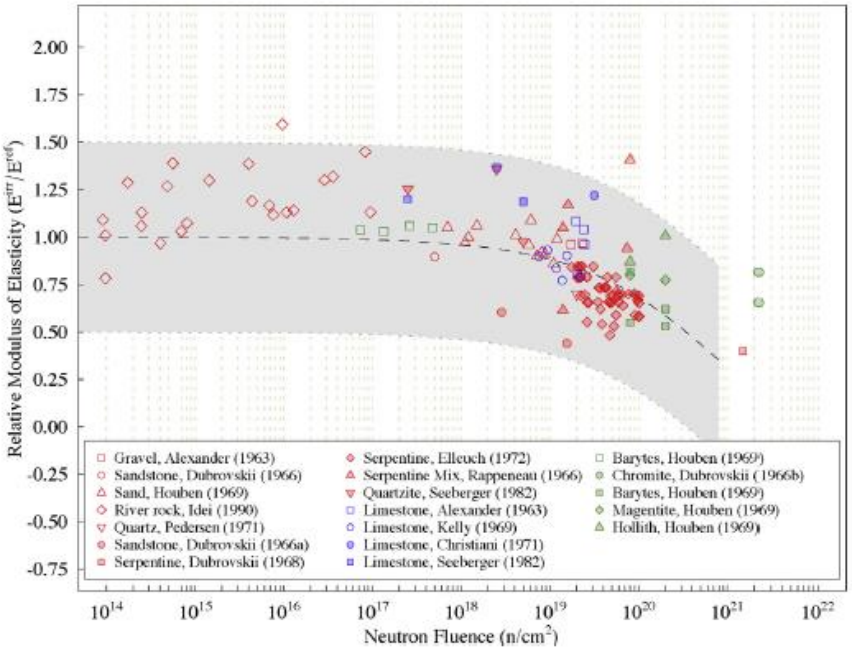

Figure 15: Relative modulus of elasticity of concrete and mortar specimens versus neutron fluence [67]

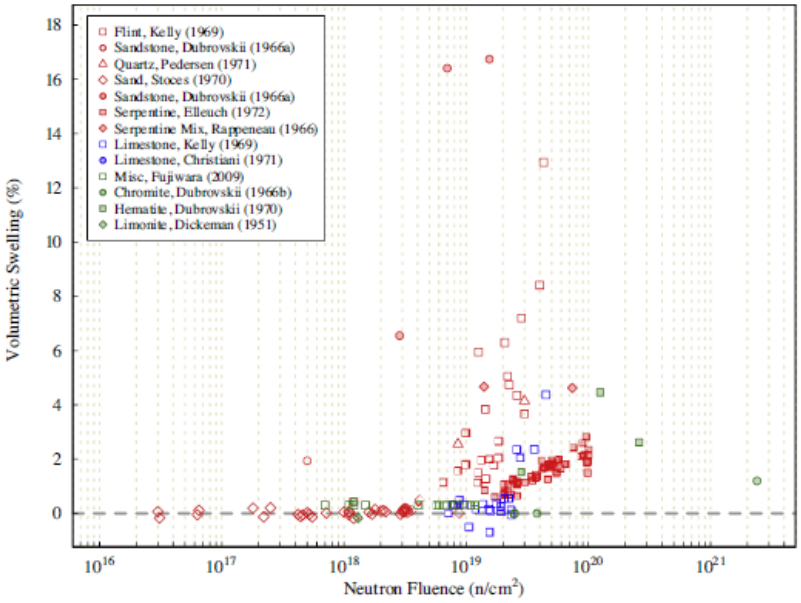

Figure 16: Volumetric swelling of concrete and mortar specimens versus neutron fluence [67]

3.3.4 Alkali-Silica reaction

In recent studies a coupling effect of alkali-silica reaction (ASR) and nuclear radiation have been recorded as a possible reason for additional swelling of concrete when compared to the known values of particular aggregate expansion due to irradiation.

Ichikawa and Koizumi [84] and Ichikawa and Kimura [85] showed that ASR nonreactive aggregates can become ASR-sensitive under irradiation, depending on the intensity of the radiation, the reactivity of the aggregate, and the alkali content in cement.

The general alkali-silica reaction is a complex set of chemical reactions between alkali cations and hydroxyl ions from concrete pore solutions. The necessary conditions are the presence of alkalis in the cement paste, reactive silica in the aggregate and moisture or water. The alkalis react with silica in the pore solution and produce an alkali-silica gel, which further absorbs moisture leading to excessive swelling. The rate and degree of these reactions depend on the temperature, type and proportions of the reacting materials, gel composition, gradation of aggregates, and other factors. The process can be described by these four steps [86]:

a) dissolution of silica by hydroxyl attack,
b) reaction of surface silanol groups with OH^-,
c) binding of cations to the silicate,
d) reaction to form calcium silicate hydrates.

The aggregate that is likely to undergo ASR are the ones containing reactive SiO_2, e.g. crystalline tridymite, cristobalite, and strained quartz; or amorphous opal, chert, and glassy volcanic materials.

However, it was found that under neutron irradiation, the degree of ASR does not correspond to the known reactivity of aggregate. For example, limestone and flint showed the same degree of expansion under neutron radiation, even though it is known, that flint aggregate is at normal conditions about five times more reactive than limestone [84]. Ichikawa and Koizumi [84] conducted an experiment monitoring the increase in quartz reactivity under irradiation. Plates of both crystalline and amorphous quartz were exposed to 200 keV Ar ions. It was found out, that at 6×10^{14} Ar/cm^2 the reactivity of crystalline quartz significantly increased. At this dose the crystalline quartz was close to amorphization, which was concluded to be a factor responsible for the rise in reactivity. But, it should be pointed out, that the increased reactivity of aggregate does not necessarily mean, that ASR will be present. It depends on many other factors stated above, especially on the chemical composition of cement. Also aggregate types, which are normally resistant to ASR may become ASR-sensitive under irradiation as it was shown by Ichikawa and Kimura [85]. A crystalline plagioclase was at a dose of

0.9×10^8 Gy of irradiation by a 30 keV electron beam converted to the amorphous state, which induced 35 times higher reactivity compared to its initial state.

Further investigations relating the ASR promoted by irradiation are needed to confirm or displace such theories and to complete them with findings relating the stiffness of the irradiation induced ASR, which determines its degree of damage to concrete.

4 Experimental programme

The topical issue of verification the safety of NPPs´ structures in relation to licences prolongation have raised a new wave of research works in many countries, which are dependent on nuclear power, playing important part of their national energy mix. Although there is a tendency to "turn green" and utilize the renewable sources as the main form of energy supply, the inconsistency of such sources and the lack of the particular conditions needed makes it an unreliable way of energy production and for some countries even an unattainable goal. Therefore, the nuclear power has its relevant importance and is supposed to become even more significant considering the gradual decline of fossil fuels use.

Various numerical models have been developed and are continuously being improved to predict the aging of the containment concrete structures, which could be very useful tool when determining the actual state of the single structures inside the containment [38]. However, no numerical model can be worked out without an input data and experimental verification. Filling the gaps of the state-of-the-art knowledge is in these days aimed at the irradiation influence on concrete, which must be carried together with studies of thermal effects, being able to conclude which phenomena were caused by the accompanying heating and set them apart. Considering the concrete of biological shielding, which is unique for its special mix composition, the effects of heating are less researched. The goal of this experimental program is to broaden the knowledge of thermal loading effects on concrete with special focus on its design representing the appropriate composition of concrete for biological shield. The conventional testing is carried together with certain common non-destructive methods in order to find correlations between the degree of concrete deterioration and its parameters easily gained using NDT, as NDT presents a powerful tool providing the monitoring of structures and its ageing process.

4.1 Composition

Prior to the design of mixtures´ composition, a preliminary study investigating the suitability of cement types for this specific application had been conducted. Commonly

used binder for biological shielding concrete is Portland cement Type I[1]. However, for BSC the internal integrity is of major importance and thus any rise of cracks due to hydration heat or drying shrinkage is highly undesirable. For this reason, blended cement was supposed to perform better. Portland blast furnace slag cement CEM II/B S 32.5 (CEMEX Cement, k. s., Prachovice) was selected to be compared with Portland cement CEM I 42.5 R (Českomoravský cement, a. s., Mokrá) in regard to its volume changes during hydration next to the compressive and flexural strength. Two sets of specimens were prepared to study the development of these properties in time, each set exposed to different curing regimes – on air in laboratory conditions and under water. CEM II/B-S 32.5 showed significantly better performance in the means of volume changes for both curing regimes as well as in the means of mechanical properties and therefore it was selected as the binder component for the mixtures of BSC. Results of the preliminary study can be found in [87].

Five types of aggregate were selected as the typical suitable aggregate used for biological shielding concrete: *serpentine* for its high content of chemically bound water and as a representative of BSC of the Czech power plant Temelín; *barite* and *magnetite* as the most suitable and available types of heavy weight aggregate; *basalt* for its superior performance under elevated temperatures; and *limestone* as cheaper and easily accessible alternative and as the representative aggregate of concrete structures of the Slovak power plant Jaslovské Bohunice. Aggregate basic characteristics and information about the supplier are given in Table 9.

Table 9: Characteristics of used types of aggregate

Aggregate type	Density [kg/m^3]	Supplier	Approx. cost without VAT [EUR/t]
Serpentine	2 670	SHB, s.r.o Bernartice 97, Czech Republic	8.3
Barite	4 100	Sachtleben Bergbau GmbH & Co. KG in Hausach, Germany	290.0
Magnetite	4 800	LKAB Minerals, LULEÅ Sweden	200
Limestone	2 700	Kamenolomy ČR, Řeporyje Prague 5, Czech Republic	9.0
Basalt	3 000	KÁMEN Zbraslav a.s, Dobkovičky, Litoměřice, Czech Republic	8.5

[1] The classification of cement types in this thesis is always in accordance with national standard, i.e. ČSN EN 206-1 Concrete - Part 1: Specification, performance, production and conformity [23]

The granulometry of each aggregate type was determined separately to achieve good workability in accordance with the ideal grading curve using the data from sieve analyses supplied by manufacturers. The achieved granulometries after the determination of suitable weight ratios is shown in Figure 17. The amount of cement, water and plasticizer is the same for all mixtures to enable direct evaluation of the aggregate type influence. The exceptional higher amount of water in case of limestone was due to its high water absorption. The final composition of studied mixtures is presented in Table 10.

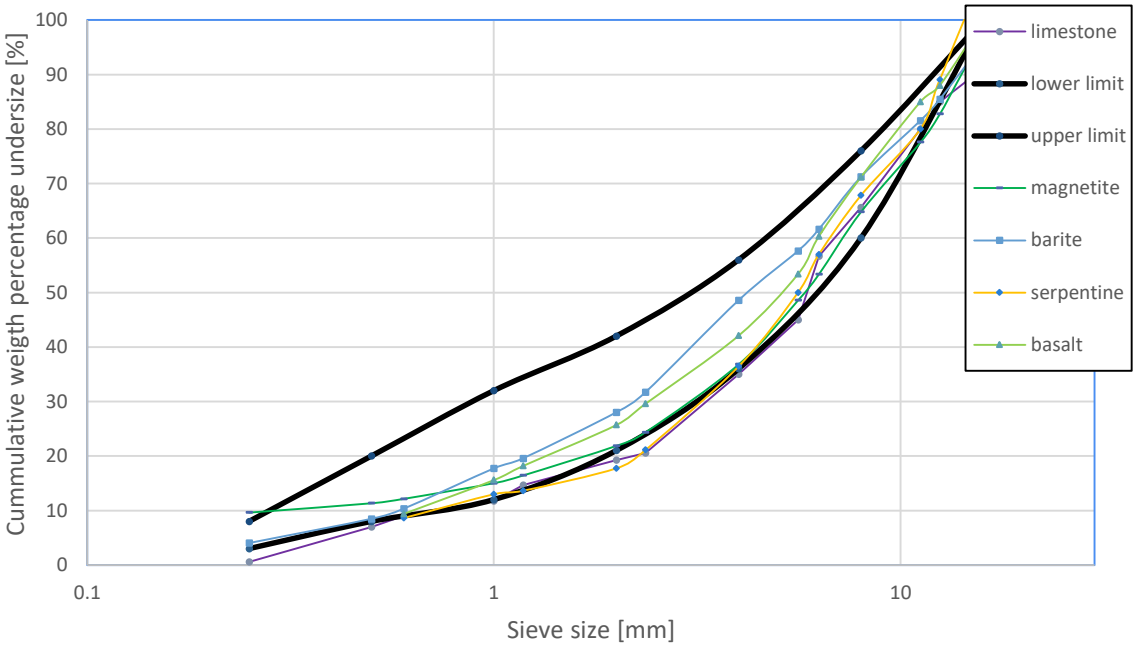

Figure 17: The granulometries of used types of aggregate

Table 10: The mixture composition of studied biological shielding concrete types

Label	Binder constituent	Amount [kg/m^3]	Aggregate type	Fraction	Amount [kg/m^3]
SC_Ba	Cement CEM II/B-S 32.5	400	Barite	0 – 2	197
	Water	200		1 – 8	507
	Plasticizer Stacheplast	4		0 - 16	2110
SC_M	Cement CEM II/B-S 32.5	400	Magnetite	0 - 8	1286
	Water	200		0 - 20	1930
	Plasticizer Stacheplast	4			
SC_S	Cement CEM II/B-S 32.5	400	Serpentine	0 - 4	1078
	Water	200		4 - 8	180
	Plasticizer Stacheplast	4		8 - 16	539
SC_B	Cement CEM II/B-S 32.5	400	Basalt	0 - 4	1166
	Water	200		4 - 8	194
	Plasticizer Stacheplast	4		8 - 16	583
SC_L	Cement CEM II/B-S 32.5	400	Limestone	0 - 4	1085
	Water	229		4 - 8	181
	Plasticizer Stacheplast	4		8 - 16	543

4.2 Specimens manufacture

The manufacture of concrete samples was carried out in stages due to the large number of samples contradicting the limited number of moulds and difficult handling of the high volumes of fresh concrete, especially when high-density aggregate was used. Five sets of samples were prepared during one week period, which was enough to proceed with manufacture, curing of samples and demoulding. The mixing procedure itself followed the national standard ČSN EN 12390-2 [88], as the prepared aggregate in fractions of calculated ratios were mixed first, followed by the addition of cement and after the thorough mixing of the dry constituents, water with plasticizer were added and mixed until a proper consistency of the fresh concrete was achieved. The produced samples were of normalized shape and dimensions: cubes in size of 150 mm per side and prisms with dimensions of 100 x 100 x 400 mm [89]. The samples were cured in laboratory conditions on air for the specified time periods before testing or thermal treatment. All procedures were conducted in the technological laboratory of the Experimental Centre of the Faculty of Civil Engineering of the Czech Technical University in Prague.

Figure 18: Samples preparation – example of one out of the five sets – Barite concrete

4.3 Methodology of testing procedures

Part of the prepared specimens was tested prior to thermal treatment for the sake of reference, both destructively and with the use of NDT methods in the age of 28 days and 90 days. Thermal treatment was performed on the 90-days old specimens, which were firstly dried in a desiccator at 105°C and either tested after drying or exposed to 200°C or to 400°C for two hours. After the heat treatment, the samples were placed back

into the desiccator to cool to lower temperature, then sealed with a plastic foil to enable cooling to room temperature but to avoid the intake of any water vapour. Prisms were tested with NDT techniques at all stages of thermal treatment, i.e. after drying, after the exposition to 200°C and to 400°C. After the final heating stage, they were finally tested destructively using the three-point bending test method with the record of the loading procedure. The samples were also measured and weighed prior testing in order to calculate changes in bulk density. Cubes were tested in all stages destructively through compressive strength test.

4.3.1 NDT techniques

Ultrasonic impulse testing method

Ultrasonic impulse testing method (US method), according to ČSN 73 1371 [90], was used to determine the dynamic Young´s modulus of elasticity in the reference state and after thermal treatment as an indicator of deterioration of concrete and also served as the first estimate of expected frequency for resonance method (see further). The measurement is based on the ultrasonic wave passage through the sample, which is emitted through a probe (transmitter) and received by another probe (receiver). The parameters of wave motion are dependent on the properties of the material, which it passes through, therefore it enables to indicate the degree of concrete degradation, estimate Young´s modulus of elasticity, strength or other parameters. The frequencies of ultrasonic waves used in civil engineering are 20 – 150 kHz, which can pass through thick layers of material. For good contact of the probe with the studied material an appropriate agent has to be used, such as a plasticine or a special conductive gel used for sonography. For different purposes, the set of the testing varies, as it can be used both in laboratory for prepared specimens or on site for real structures. In certain cases, the receiver and transmitter are integrated within one probe using the wave reflection from the other surface of the concrete block. The set-up of performed measurement for the determination of dynamic Young´s modulus in laboratory conditions on prisms illustrated in Figure 19. In this case, the signal velocity v is proportional to the trajectory and is calculated using the basic formula:

$$v_L = \frac{l}{t} \qquad (5).$$

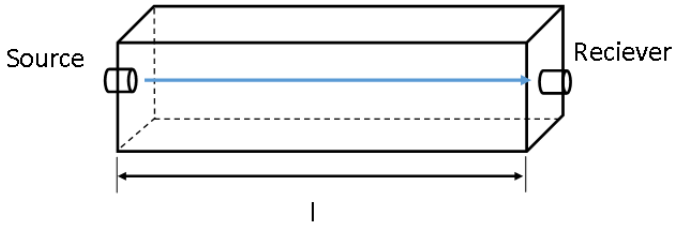

Figure 19: Set-up of ultrasonic impulse method

The measurement was performed with the use of Pundit Lab Plus^{+} device manufactured by Proceq SA three times for each sample, calculating the velocity as the arithmetical average. The dynamic Young´s modulus of elasticity E_{cu} was then calculated:

$$E_{cu} = \rho \, v_L^2 \, \frac{1}{k^2} \quad (6),$$

where ρ is the sample bulk density [kg/m^3] and k is the ambient dimensionality ratio, which depends on the minimum specimen dimension of the sample and the Poisson´s ratio μ_{cu}.

Ambient dimensionality ratio for 1D, 2D and 3D respectively was calculated as follows:

$$k_1 = 1 \quad (7)$$

$$k_2 = \sqrt{\frac{1}{1-\mu_{cu}^2}} \quad (8)$$

$$k_2 = \sqrt{\frac{1-\mu_{cu}}{(1-\mu_{cu})-(1-2\,\mu_{cu})}} \quad (9).$$

Criteria for determining the dimensionality provided by the standard:

1) 1D (for bars, beams etc.)
   $a \leq 0.2\ \lambda_L$
2) 2D (for thin slabs)
   $t \leq 0.2\ \lambda_L$
3) 3D (for bars, prisms, cylinders, beams)
   $a \geq 2\ \lambda_L$
   $b \geq 2\ \lambda_L$,

where a, b are the dimensions orthogonal to the direction of wave propagation [m], t is the width of a slab [m] and λ_L is the wavelength of the ultrasound impulse.

Resonance method

The principle of resonance method is measuring the eigenfrequencies during longitudinal, transversal and torsional oscillation, which characterize the dynamic behaviour of concrete. From the measured frequencies the physico-mechanical properties can be calculated, such as dynamic modulus in tension, compression and shear and as well Poisson´s ratio. Afterwards, the degree of degradation can be determined studying the changes in the measured or calculated values.

The testing procedure was performed according to ČSN EN 73 1372 [91]. The specimens were placed on a base, which did not constrain the sample´s oscillation movements and its eigenfrequency varied from the eigenfrequency of the sample. After excitation of the mechanical oscillation the signal was recorded through a transducer, digitalized and saved as a voltage-time record. Afterwards, the saved data were transformed to amplitude vs. frequency plot (spectrum) using Matlab software. The sought eigenfrequncies appeared as peaks in the frequency spectrum. The set-up and calculations differed for longitudinal, transversal and torsional oscillation.

Longitudinal oscillation

The specimen was placed on a support in the node, which is the place of zero movements during oscillation - in this case in the centre of its length, to enable free longitudinal oscillation. Transmitter and receiver were placed on the opposite sides of the sample in the direction of its longest side, as shown in Figure 20.

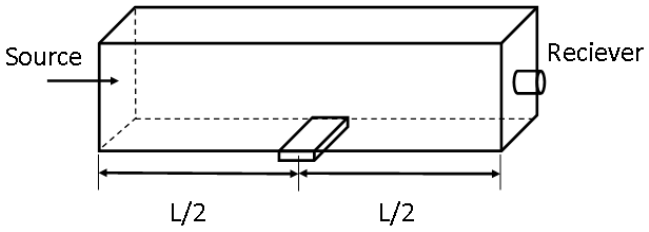

Figure 20: Scheme of longitudinal oscillation

The Young´s modulus of elasticity in the longitudinal direction E_{crL} [MPa] was then calculated using the formula:

$$E_{crL} = 4\,L^2 f_L^2 \rho \qquad (10),$$

where L is the length of the sample [m], ρ is bulk density of the sample [kg/m^3] and f_L is the first eigenfrequency of longitudinal oscillation.

Transversal oscillation

The specimen was placed on two supports located in the nodes of zero movements, as shown in Figure 21. The positions of oscillation source and the receiving transducer were on the same side of the sample in the location of the neutral axis.

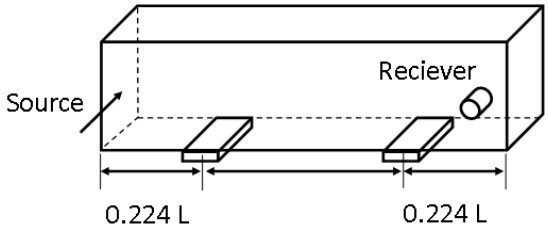

Figure 21: Scheme of transversal oscillation

The calculation of Young´s modulus of elasticity in the transversal direction E_{crf} [MPa] was made as follows:

$$E_{crf} = 0.0789\, c_1\, L^4 f_f^2 \rho\, \frac{1}{i^2} \quad (11),$$

where L is the length of the sample [m], ρ is bulk density of the sample [kg/m^3], f_f is the first eigenfrequency of transversal oscillation, i is the gyration radius and c_1 is a corrective coefficient, which involves the influence of shear and moment of inertia and is dependent on the slenderness.

Torsional oscillation

The lay-out of torsional oscillation measurement is presented in Figure 22 with the position of the support and both source and receiver of the oscillation.

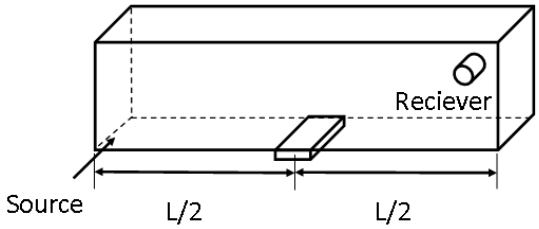

Figure 22: Scheme of torsional oscillation

The shear modulus of elasticity G_{cr} [MPa] in the direction of torsion was determined using the formula:

$$G_{cr} = 4\, k\, L^2 f_t^2 \rho \quad (12),$$

where L is the length of the sample [m], ρ is bulk density of the sample [kg/m^3], f_t is the first eigenfrequency of torsional oscillation and k is a coefficient characterizing the shape of cross-section of the sample (for prisms with square foot: k = 1.183).

Poisson´s ratio

The determination of Poisson´s ratio was calculated with the use of the known Young´s modulus of elasticity and shear modulus of elasticity as follows:

$$\mu_{cr} = \frac{1}{2}\left(\frac{E_{cr}}{G_{cr}} - 2\right) \quad (13).$$

Logarithmic decrement

Logarithmic decrement as a measure of damping was determined with the use of the output data from Matlab software from longitudinal oscillation measurement. Resonance frequency f_{max} and the corresponding amplitude u_{max} were found, which was needed for the determination of frequencies f_1 and f_2 as the corresponding frequencies to amplitudes $u_{1/2}$ (as illustrated in Figure 23):

$$u_{1/2} = \frac{u_{max}}{\sqrt{2}} \quad (14),$$

knowing these parameters, the logarithmic decrement was then calculated as:

$$\delta = \pi \frac{f_2 - f_1}{f_{max}} \quad (15).$$

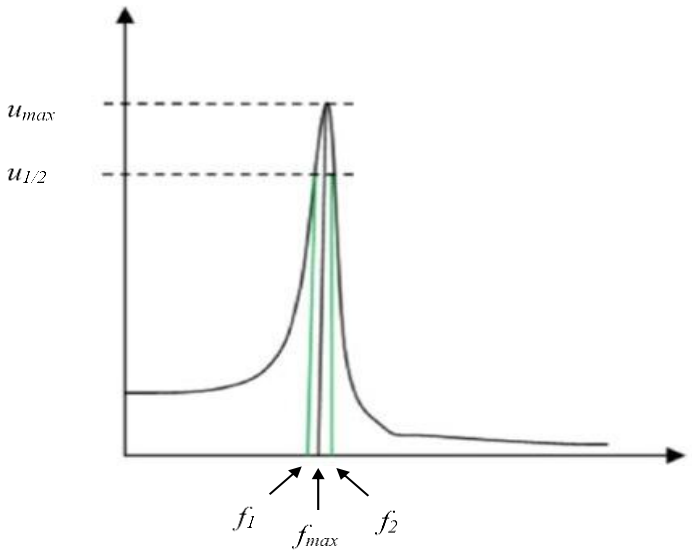

Figure 23: Determination of frequencies f_1 and f_2 from the resonance curve

4.3.2 Destructive tests

Compressive strength test

The uniaxial compressive strength test was carried out on cubes of dimensions 150 x 150 x 150 mm with the use of EDB400 following the methodology of ČSN EN 12390 [92]. The samples were loaded with constant rate of 0,2 MPa/s until rupture. The maximum load F_{max} was recorded and compressive strength *fc* was afterwards calculated as follows:

$$f_c = \frac{F_{max}}{S} \quad (16),$$

where *S* is the cross-section area of the cube sample.

Three-point bending test

To determine the flexural strength three-point bending test was performed according to ČSN EN 12390-5 [93]. The sample was placed in a steel jig with two strain indicators and a load cell was used for the stress-strain relationship record during the loading of the sample until rupture. The loading rate was in the range of 0.04 – 0.06 MPa/s. Knowing the maximum load F_{max} and the dimensions of sample, the flexural strength was then calculated:

$$f_{cf} = \frac{3\,F_{max}\,l}{2\,h\,d^2} \quad (17),$$

where *l*, *h* and *d* are the dimensions of the sample as shown in the Figure 24.

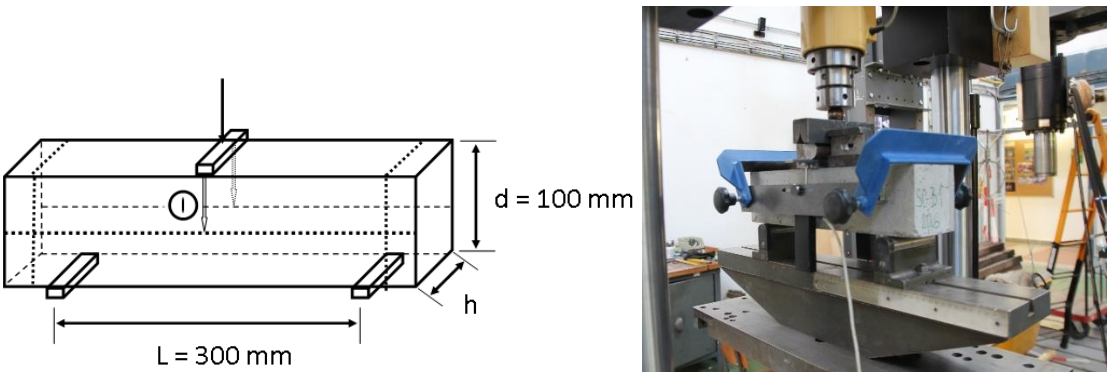

Figure 24: Scheme and the layout illustration of three-point bending test

The recorded stress-strain relationship was afterwards used for the determination of the static modulus of elasticity in tensile bending, which was calculated from its linear part, which refers to the elastic state of concrete. The modulus of elasticity calculated

using relationship, which was derived from the known formula of beam deflection *w* [m] according to Kirchhoff´s theory[2] under three-point bending test given here:

$$w = \frac{F\,L^3}{48\,E\,I} \quad (18),$$

where *F* is the load in the elastic state of concrete (determined in 1/3 of maximum stress) [N], *L* is the span length [m], E is the static modulus of elasticity [MPa] and *I* is moment of inertia [m^4] calculated from the samples cross-section with width *b* [m] and height *h* [m]:

$$I = \frac{b\,h^3}{12} \quad (19)$$

Static modulus of elasticity E was therefore calculated using the following formula:

$$E = \frac{F\,L^3}{48\,w\,I} \quad (20).$$

4.4 Discussion of results

The chapter provides results of the listed tests including discussion of obtained values. Each presented value, characterizing particular property of particular concrete type, was achieved as an arithmetical average from three measurements performed on three different samples in order to exclude major measurement errors.

4.4.1 Physical and mechanical properties before thermal treatment

All studied properties were determined after 28 and 90 days from specimens manufacture to compare the characteristics of studied concrete types in normal (laboratory) conditions, i.e. before thermal treatment. Bulk density, compressive and flexural strength, static modulus of elasticity were achieved from destructive testing, while dynamic modulus of elasticity, shear modulus, Poisson's ratio and logarithmic decrement were obtained through NDT. Each graph in this sub-chapter is presented in absolute values with the display of error bars. The error bar represents the interval of twice the value of standard deviation calculated from values obtained from the measurements on three different specimen for each concrete mixture.

[2] Considering the geometry of specimens, more precise determination of beam deflection would be with the use of Mindlin´s theory, which includes the influence of shear. However, to enable direct calculation of static modulus of elasticity, the influence of shear was neglected.

Destructive tests

Figure 25 presents the values of bulk density and compressive strength of studied concretes. The highest bulk density was achieved with the use of magnetite aggregate followed by barite aggregate, which was in accordance to the densities of the aggregate themselves. Compressive strength of all studied concrete types varied within 37 – 45 MPa at 28 days. Good performance was achieved for basalt, limestone and magnetite concrete, even though in case of limestone there was additional water incorporated in the mixture due to the aggregate high absorption. Barite and serpentine on the other hand showed slightly lower values, although barite aggregate was expected to perform better being the most expensive aggregate type used in the experiment. Flexural strength and static modulus of elasticity are presented in Figure 26. Flexural strength showed similar trends as in case of compressive strength, although it should be noted that the measurement errors are much higher than in case of compressive strength and thus the variations are not very significant. However, the poor behaviour of barite concrete is clearly visible – such difference in values compared to other concretes is not within the scale of measurement error. There were also high variations in the values of static modulus of elasticity revealing no exact trend, but once again showing the lowest values for barite concrete.

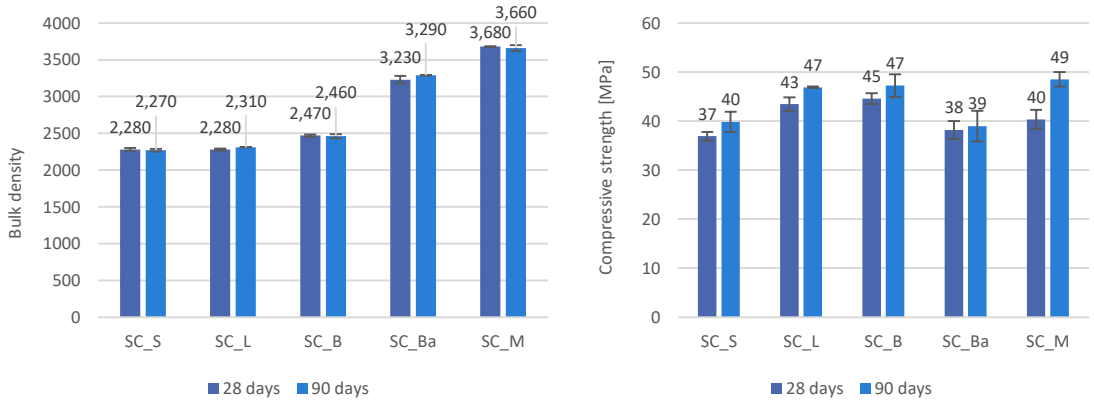

Figure 25: Bulk density [kg/m^3] and compressive strength [MPa] of studied concretes after 28 and 90 days from manufacture

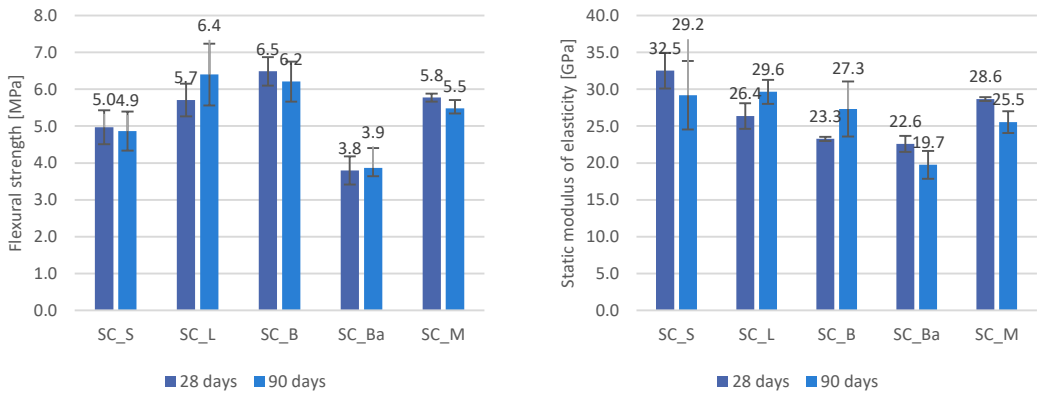

Figure 26: Flexural strength [MPa] and static modulus of elasticity E [GPa] of studied concretes after 28 and 90 days from manufacture

Non-destructive tests

The example of output of data processing in Matlab in graphs is presented in Figure 27. Matlab was used for gaining the needed eigenfrequencies (in longitudinal, transversal and torsional direction) for the calculation of parameters to be obtained using resonance method. The graphs present the dependence of deflection over time (a) and its dependence on frequency, i.e. spectrum (b). Due to the large number of obtained graphs, the figure presents only one example of studied materials (magnetite concrete) achieved after measurement after 28 days from manufacture. All data were then evaluated and summarized in column graphs presented below.

Figure 28 presents the values of dynamic modulus of elasticity obtained from ultrasound impulse method - E_{cu} and from resonance method measuring longitudinal oscillation – E_{crL}. Values measured by ultrasound method are slightly higher, but generally follow the same trend as in case of values from the resonance measurement. The best performance was recorded for magnetite concrete; limestone and basalt came after. Serpentine and mainly barite once again showed the lowest values of studied materials. Values of modulus of elasticity achieved from transversal oscillation E_{crf} during resonance method measurement and shear modulus G_{cr} are given in Figure 29 and approves the above mentioned trends. Calculated Poisson´s ratio and logarithmic decrement are presented in Figure 30. Poisson´s ratio varied between 0.27 – 0.31, but results showed high scatter, which is manifested by the wide scale of error. Logarithmic decrement, which gives information about the damping characteristics of the material, was found to be the highest in case of serpentine concrete, reaching twice the value of

barite concrete. This characteristic was however observed mainly for later evaluation of its changes after thermal treatment, as it is a good indicator of internal material damage.

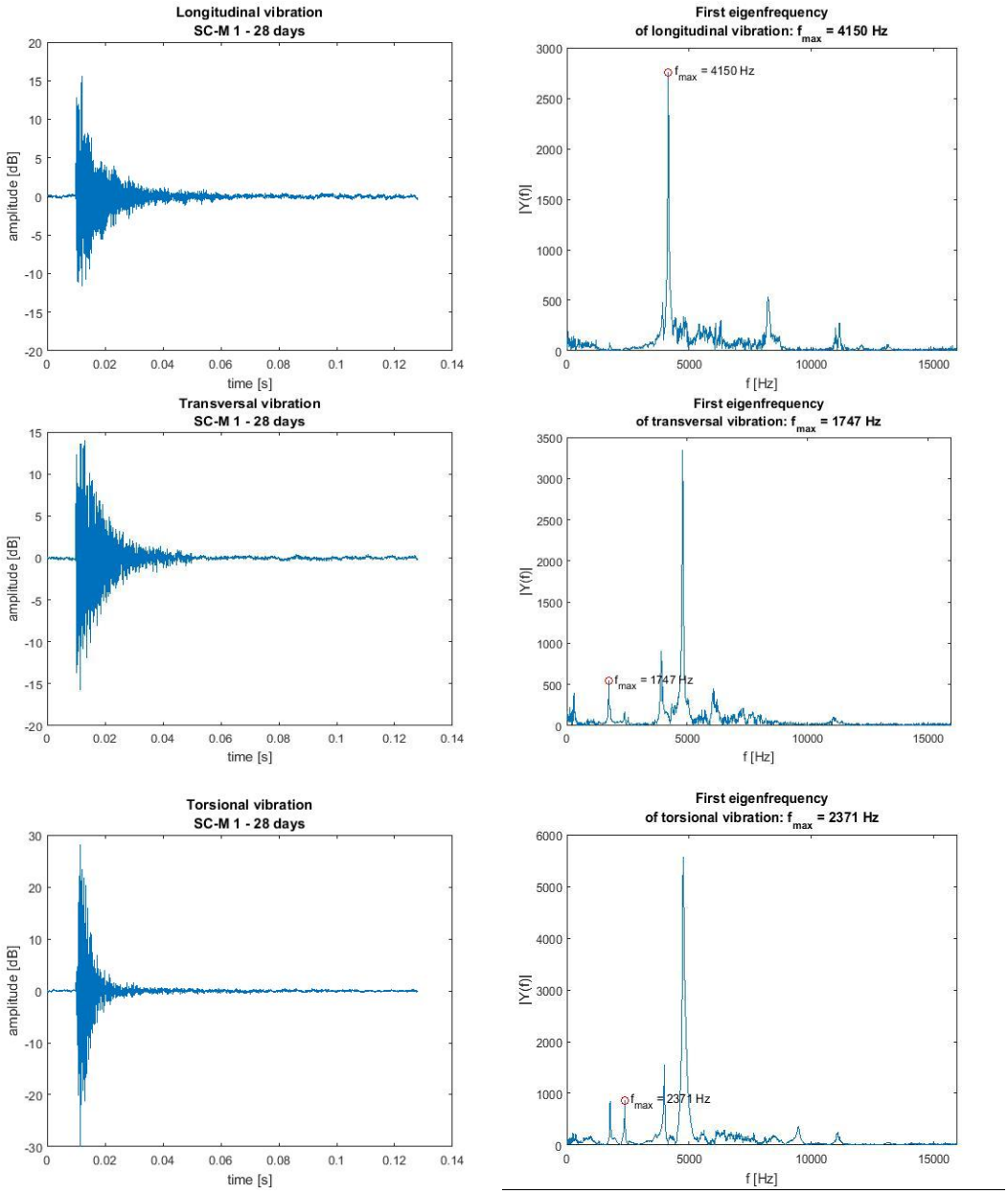

Figure 27: Example of output from data processing using Matlab software. Graphs refer to magnetite concrete measured by resonance method in longitudinal, transversal and torsional direction. Left graphs shows the dependency of deflection on time, right graphs display the spectrum of the oscillation with marked eigenfrequencies.

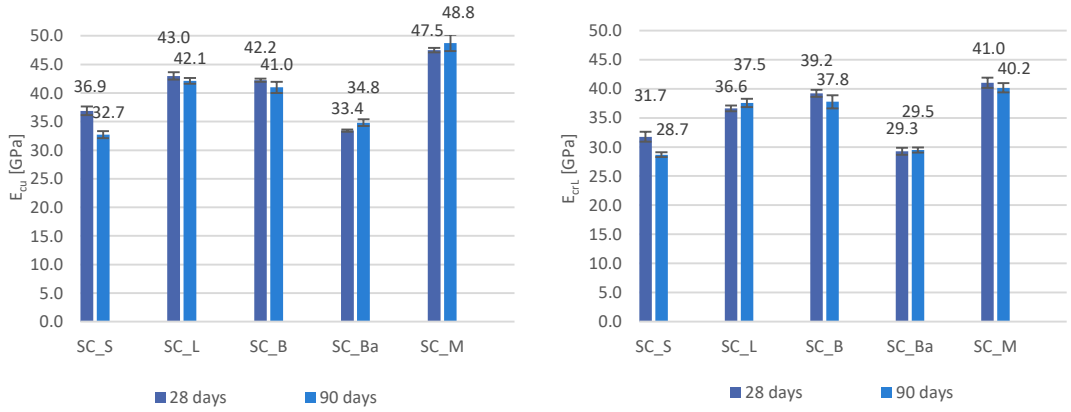

Figure 28: Dynamic modulus of elasticity obtained from ultrasound impulse method E_{cu} [GPa] and dynamic modulus of elasticity obtained from resonance method in longitudinal oscillation E_{crL} [GPa]

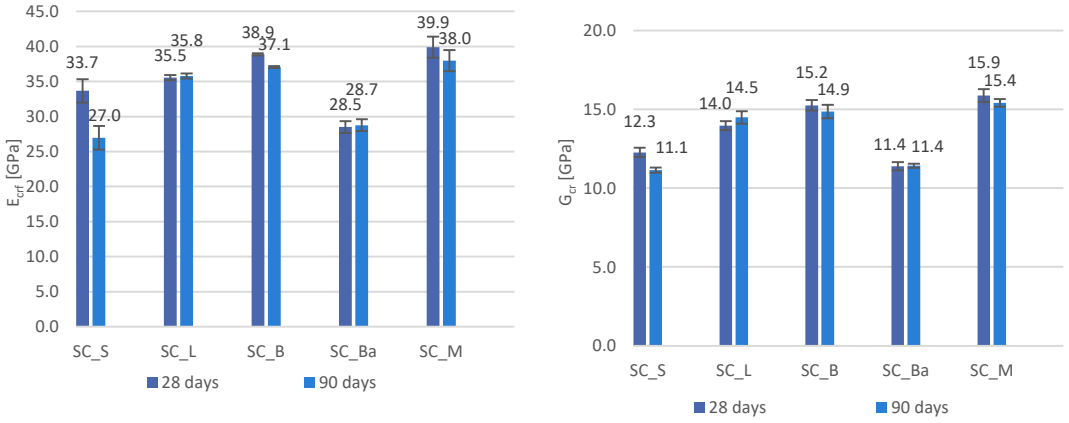

Figure 29: Dynamic modulus of elasticity obtained from resonance method in transversal oscillation E_{crf} [GPa]and shear modulus of elasticity G_{cr} [GPa]obtained from resonance method

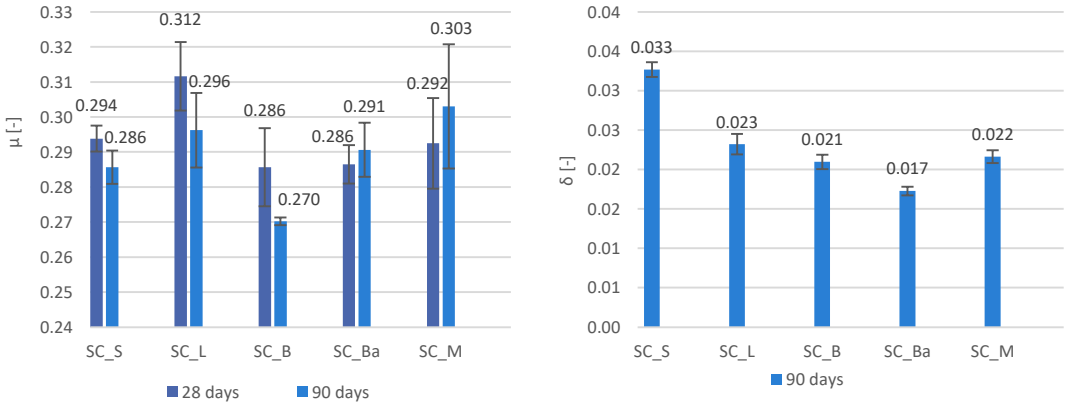

Figure 30: Poisson´s ratio μ [-]and logarithmical decrement δ [-]obtained from resonance method

4.4.2 Changes of properties due to thermal treatment

This sub-chapter evaluates the influence of three stages of concrete samples´ thermal treatment – after drying at 105°C and after the exposition to 200°C and to 400°C for two hours in both stages. The results are presented as relative values referring to the values measured after 90 days before thermal treatment, which were taken as reference.

Destructive tests

Due to the limited number of specimens, the destructive tests on prisms (flexural strength and static modulus of elasticity) were performed only after heating at 400°C. On the other hand, cubes were tested in all stages of thermal treatment, which gave the whole picture of compressive strength changes.

Relative values of compressive strength at all stages of heating as well as reference values of non-heated samples are given in Figure 31. Except from serpentine concrete there is a drop in values after drying of samples at 105°C, but the values further rose after the exposition of samples to 200°C. This is in agreement with the graph of Kaplan´s compilation work presenting dependence of compressive strength of concrete on temperature (see in Chapter 3.2.2) and it is probably caused by the additional hydration of unreacted particles in concrete driven by the force of escaping water vapour. Serpentine concrete behaved differently showing higher values in all stages of heating compared to reference values, which is quite possible performance considering the results of other studies reported in literature [42]. The decrease in compressive strength after the final stage of heating, i.e. to 400°C, was within 20% except from barite concrete. The drop to 66% of the initial value shows, that barite concrete was not well resistant to high temperatures and although it was expected to show good performance considering its high cost, it turned out to be the least suitable for the purpose of BSC in the thermal resistance point of view.

Figure 32 presents relative values of flexural strength (left) and static modulus of elasticity (right) obtained from the three-point bending test. The highest drop in values of flexural strength was found for barite concrete, after heating to 400°C reaching only 19% of the initial value. Contrary, serpentine concrete performed much better under the exposition to heat, maintaining 77% of its initial flexural strength. Results of static modulus of elasticity were much more balanced. The residual values ranged between 45 – 66% and thus the highest value of magnetite concrete and lowest of limestone

concrete did not show such remarkable difference as in case of flexural strength, compressive strength or other measured parameters (see further).

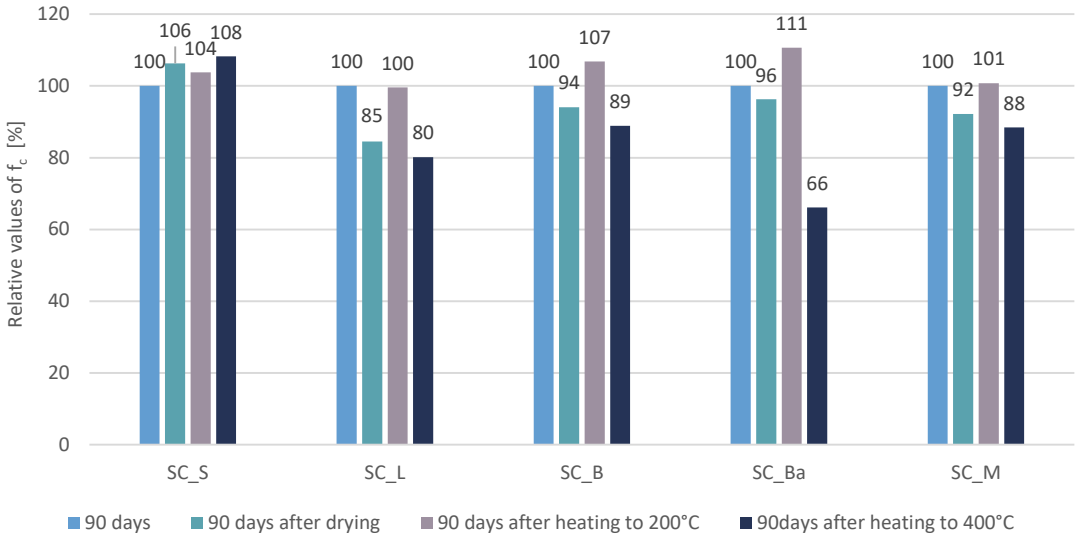

Figure 31: Relative values of compressive strength

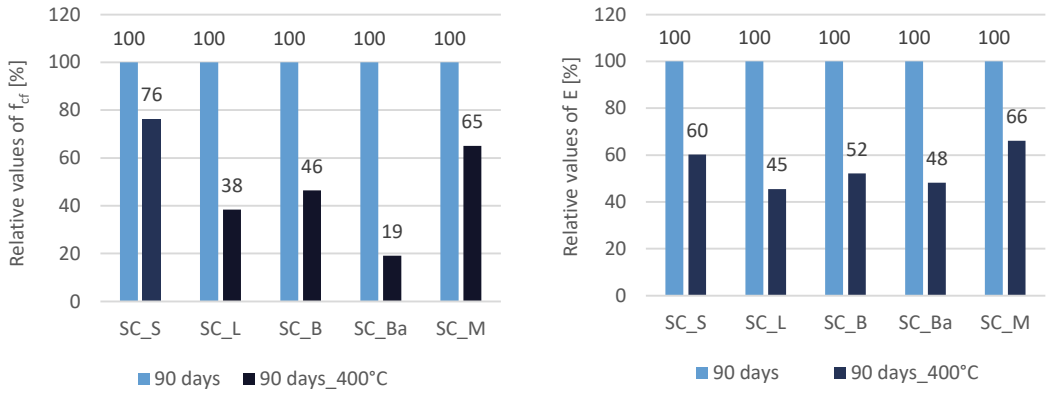

Figure 32: Relative values of flexural strength (left) and static modulus of elasticity (right)

Non-destructive tests

Figure 33 presents an example of obtained graphs after data processing in Matlab in all stages of thermal treatment. As previously, due to its large number, only longitudinal oscillation for one specimen is displayed.

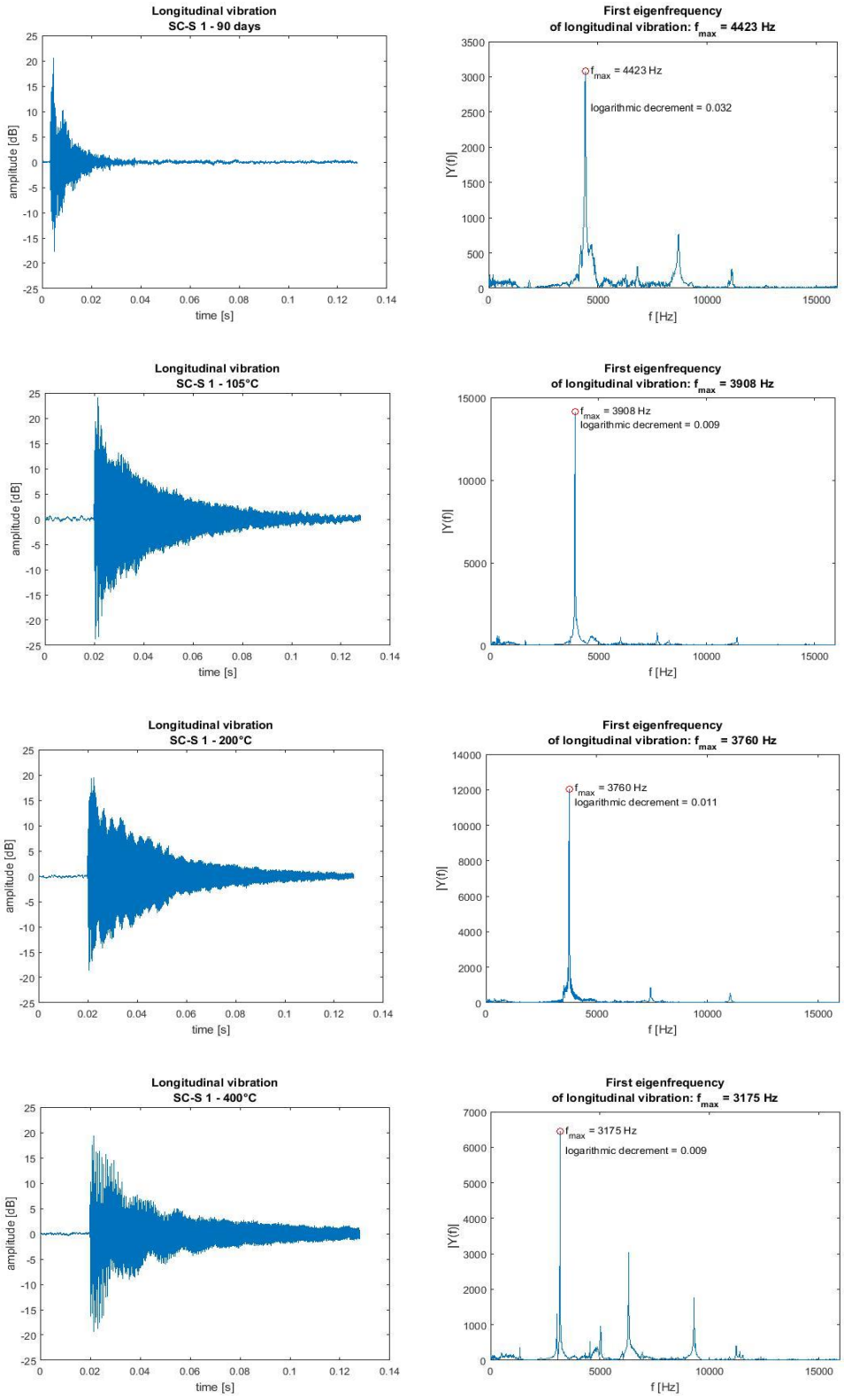

Figure 33: Example of output from data processing using Matlab software. Graphs refer to serpentine concrete measured by resonance method in longitudinal direction in the following order: before thermal treatment, after drying, after heating to 200°C and 400°C (left: time-deflection dependence, right: spectrum).

Results obtained from ultrasonic measurement are given in Figure 34. The decrease of dynamic modulus of elasticity E_{cu} after drying varied between 20 - 36% with the highest drop found for basalt concrete. After the exposition to 200°C the further decrease in values was not remarkable - within 10%, but when heated to 400°C there was a dramatic decline. The least influenced materials were serpentine and magnetite concrete with the drops of values to 45 and 50% respectively. Contrary, barite concrete showed only 7% residual ratio of E_{cu}.

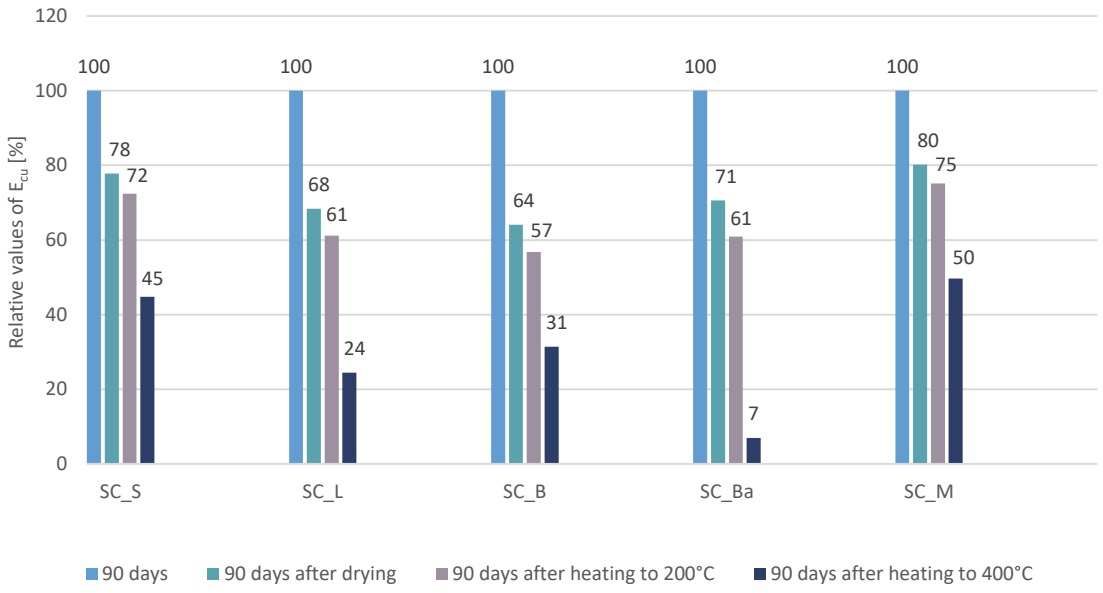

Figure 34: Relative values of dynamic modulus E_{cu} [-] of elasticity measured by ultrasound impulse method

In case of dynamic modulus of elasticity obtained from resonance method for both measurements in longitudinal (E_{crL}) and transversal (E_{crf}) directions (Figure 35 and Figure 36 respectively), the residual ratios were very similar to values obtained from US method. Only the value of barite concrete after heating to 400°C did not show such high drop but still reaching the lowest values (residual ratios of 18% and 22% for E_{crL} and E_{crf} respectively). Shear modulus (G_{cr}) residual ratios are presented in Figure 37. The best performance in the means of G_{cr} was found for magnetite concrete, which exhibited a decrease of residual ratio within 15% while exposed up to 200°C and a drop to 2/3 of the initial value after heating to 400°C and was followed by serpentine concrete. Barite, limestone and basalt concrete showed very similar values to each other in all stages of heating, reaching residual ratios after the final heating stage at about 1/3 of the original values.

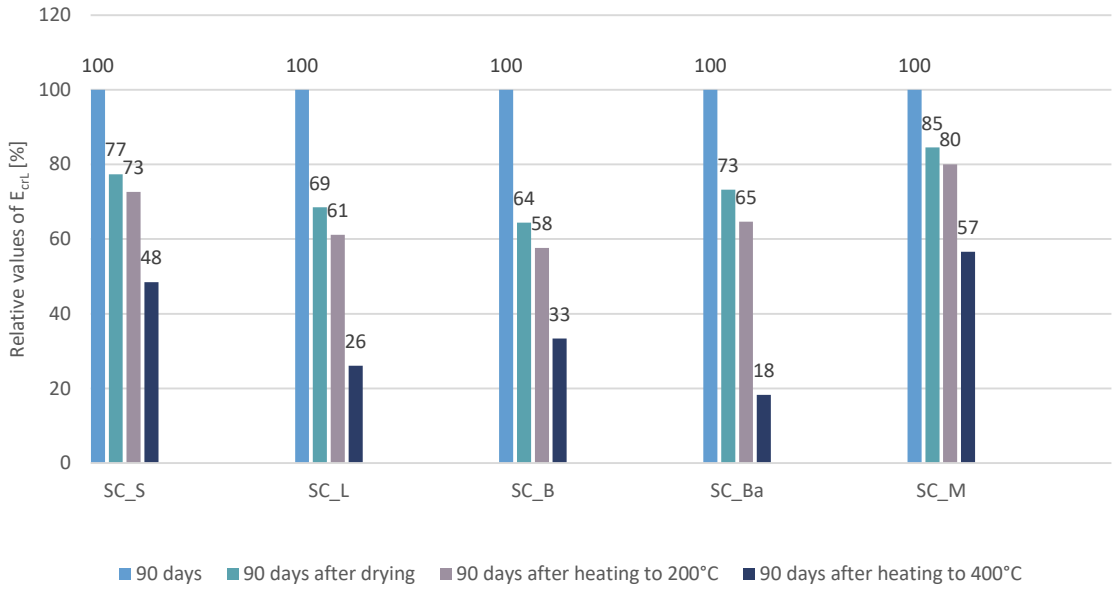

Figure 35: Relative values of dynamic modulus of elasticity measured by resonance method in longitudinal direction E_{crL} [-]

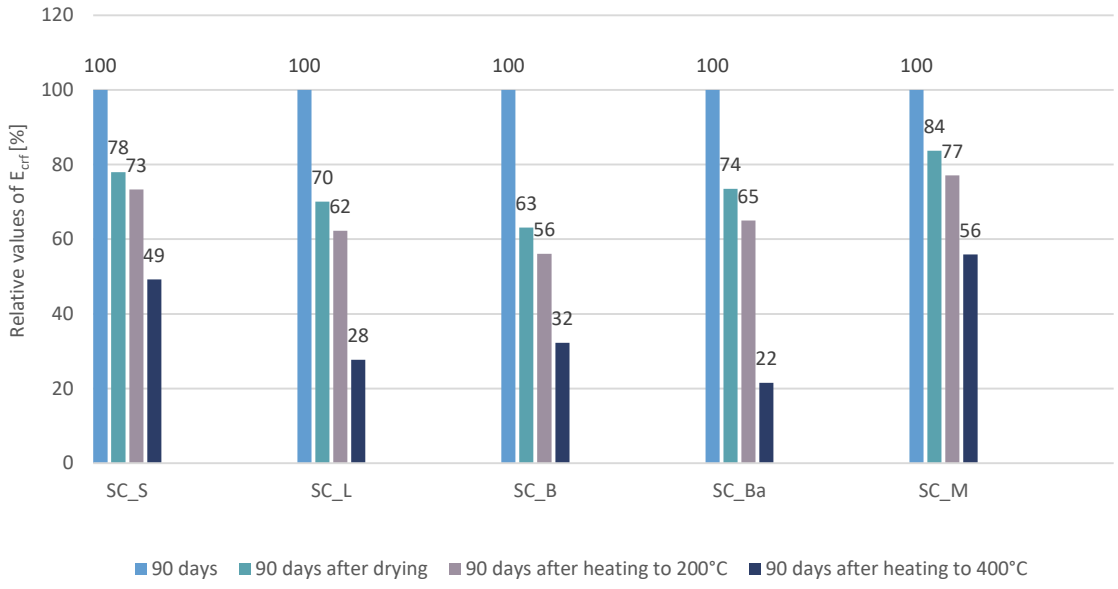

Figure 36: Relative values of dynamic modulus of elasticity measured by resonance method in transversal direction E_{crf} [-]

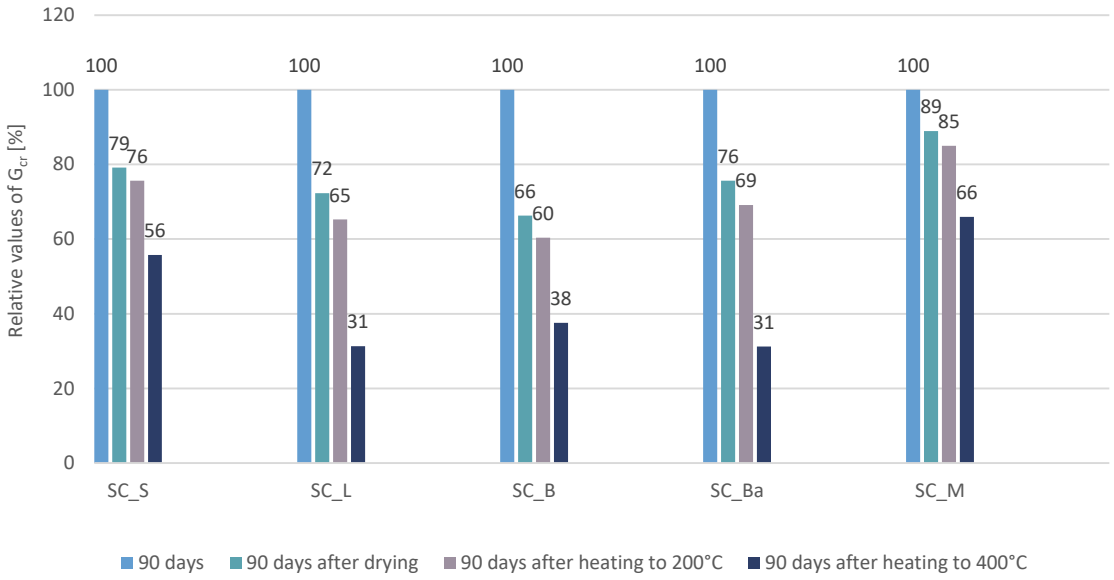

Figure 37: Relative values of shear modulus measured by resonance method G_{cr} [-]

Interesting finding was shown while evaluating results of Poisson´s ratio μ (Figure 38). The calculation of μ for barite concrete after heating to 400°C gave a negative value. This would mean, that after tensioning the transversal deformation would rise (as in case of auxetic materials - e.g. cork, special dampening matrasses etc.) contrary to normal behaviour of concrete, which exhibit transversal contraction during tensioning. The negative value was probably caused by the input data being beyond the domain of the computation formula, which may indicate, that the barite concrete internal structure experienced severe disintegration. Except barite, the lowest residual ratio of μ was found for limestone concrete – 27%, while basalt concrete showed the least decrease to 47%.

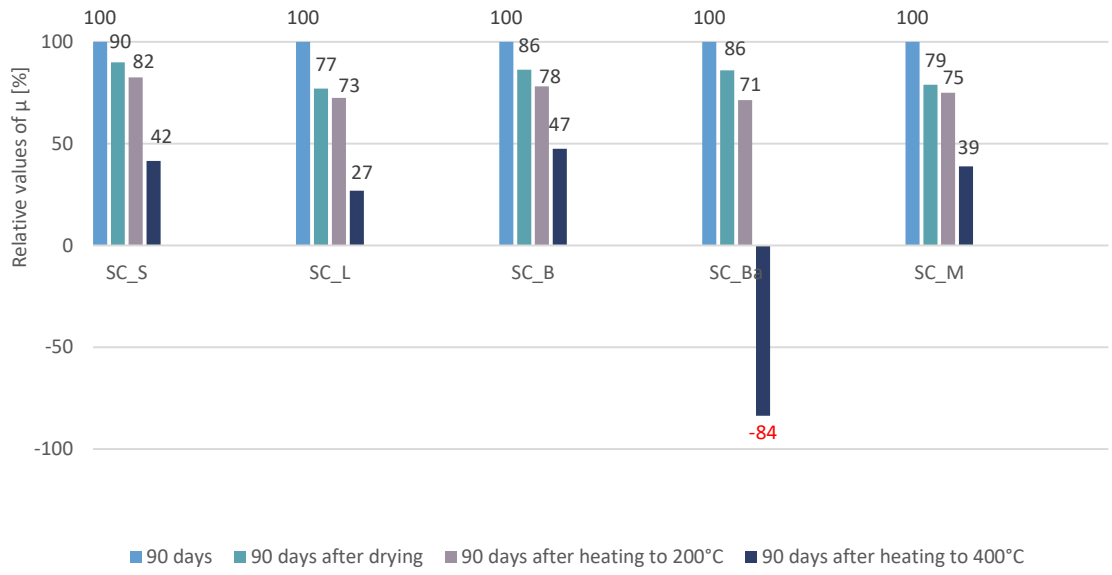

Figure 38: Relative values of Poisson´s ratio μ [-]

Figure 39 shows changes in logarithmic decrement δ. As can be seen, there was a significant drop in δ for all studied mixtures after drying. This is attributed to the loss of free water, which is a good damping material and thus its loss naturally resulted in the decrease of damping. Further increase in logarithmic decrement of the dry material is an indicator of its intrinsic damage. The oscillation in disintegrated material is highly damped due to the cracks and delaminations as some oscillating particles within the material are not in contact with the neighbouring particles and thus cannot transfer vibration energy. For the most studied materials, the logarithmic decrement did not exhibit any marked changes and in the case of magnetite concrete the values went even slightly down, which may be caused by some further escape of adsorbed water or eventually by microstructural changes. However, in case of barite concrete the logarithmic decrement very significantly increased – more than twice after heating to 200°C and nearly three times after exposition to 400°C (compared to reference values), which shows its severe microstructural damage of barite concrete, caused by the breakup of the aggregate. The bad state of specimens was visible by the naked eye, which is displayed in Figure 40.

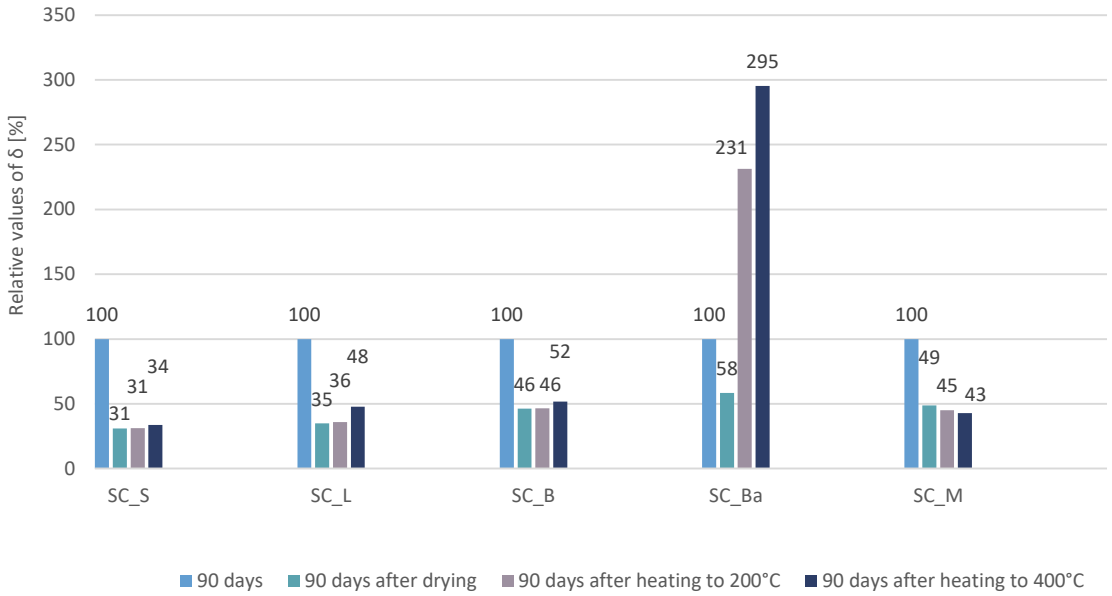

Figure 39: Relative values of logarithmic decrement δ [-]

Figure 40: Damage of barite aggregate concrete after heating to 400°C

5 Conclusion

This thesis dealt with the issue of the ageing process of biological shielding concrete mainly for the application in nuclear power plants. After the introduction to the topic, the second chapter explained the function and material composition of BSC with a very short excursion to nuclear physics for better understanding of the processes inside concrete, which is in interaction with ionising radiation. The third chapter provided the state of the art presenting the negative effects of nuclear and gamma irradiation on BSC, as well as the influence of the accompanying thermal loading. The chapter revealed gaps in the current knowledge of the topic and proposed the need of further research in this area.

The experimental program, which was presented in chapter 4, was limited to thermal loading effects on BSC due to the limited scope of the thesis, which surely could not include the highly demanding and controlled process of irradiation of any material, needing the source of ionising radiation. Five types of concrete, differing in the used aggregate suitable for biological shielding concrete, were investigated in the means of changes of their mechanical properties when exposed to elevated temperatures up to 400°C. Both destructive and non-destructive tests were conducted to create a comprehensive picture of the concrete state including its compressive and flexural strength, modulus of elasticity (both static and dynamic), Poisson´s ratio and logarithmic decrement, providing the information about internal damage. The evaluation of the concrete performance was made through direct comparison of the individual concrete types, as the choice of aggregate is the crucial factor for the biological shielding concrete resistance to irradiation. The selected types of aggregate were serpentine, being used for BSC in the Czech NPP Temelín; barite and limonite as the representatives of heavy density aggregate; basalt for its good properties when used for concrete exposed to high temperatures, and limestone for its high sources in Czech Republic and Slovak Republic, being used for concrete structures in NPP Jaslovské Bohunice.

Results showed very poor behaviour of barite concrete, which had been supposed, based on literature review, to be superior when compared to basalt or limestone. The non-destructive tests showed high disintegration of its internal structure when heated to 400°C and both flexural and compressive strength tests after heating exhibited the lowest values exactly for barite concrete. When considering the cost of the aggregate, which was the

highest from the used types, it was evaluated as the least appropriate for the use as BSC from the studied materials. On the contrary, magnetite and serpentine aggregate proved its good suitability for this application, as the recorded values of studied parameters were always superior to other materials. Basalt and limestone concrete are not very common for such special use as BSC, but could be an alternative when its source in the area is large.

Relating the compressive strength, except from serpentine concrete, there was a decrease in values when the specimens had been dried at 105°C, but after the exposition to 200°C the strength rose above the reference values. This was probably the result of additional hydration of initially unreacted cement particles, which came in contact with the escaping water. However, parameters achieved from non-destructive test showed no such trend and therefore no direct correlation between them and the mechanical parameters could be made. On the other hand, the NDT parameters showed good indication of the internal damage of concrete, which was clearly visible in the case of barite concrete, which suffered severe disintegration of aggregate when heated to 400°C.

Non-destructive testing presents a powerful tool to obtain information about the state of the real concrete structures inside containment. The further research will therefore focus on the development of new and more precise methods of NDT, which could be in future utilized during the process of licencing the prolongation of NPP operation life.

6 Literature

[1] Oak Ridge National Laboratory. Nuclear Science and Technology Interaction Programme. **2011**.

[2] Ageing Management of Concrete Structures in Nuclear Power Plants. INTERNATIONAL ATOMIC ENERGY AGENCY **2016**, 355.

[3] Bertero, V.V.; Polívka, M. Influence of Thermal Exposures on Mechanical Characteristics of Concrete. Amer. Conc. Inst. Special Publications SP34 - Concrete for Nuclear Reactors **1972**, 505-31.

[4] Fillmore, D.L. *Literature Review of the Effects of Radiation and Temperature on the Aging of Concrete*.; Bechtel BWXT Idaho, LCC: Idaho National Engineering and Environmental Laboratory, 2004.

[5] Thelandersson, S. Effect of High Temperatures on Tensile Strength of Concrete. Lund Institute of Technology **1971**.

[6] Blundell, T.; Diamond, C.; Browne, R.G. The Properties of Concrete Subjected to Elevated Temperautres. CIRIA Underwater Engineering Group **1976**, *9*.

[7] Lankard, D.R.; Birkimer, D.L.; Fondriest, F.; Snyder, M.J. Effects of Moisture Contents on the Structural Properties of Portland Cement Concrete Exposed to Temperatures Up to 500°F. Amer. Conc. Inst. Special Publication **1972**, *25*, 55-102.

[8] Lee, J.; Xi, Y.; Willam, K. Properties of Concrete After High-Temperature Heating and Cooling. ACI Materials Journal [H.W. Wilson - AST] **2008**, *105*, 334.

[9] Marechal, J.C. Thermal Conductivity and Thermal Expansion Coefficients of Concrete as a Function of Temperature and Humidity. Ibid. - Paper SP34-49 **1972**, 1047-57.

[10] Graves, H.; Le Pape, Y.; Nuas, D.; Rashid, J.; Saouma, V.; Sheikh, A.; Wall, J. Expanded Material Degradation Assessment (EMDA). Technical Report NUREG/CR-7153, ORNL/TM-2011/545. U.S. Nuclear Regulatory Commission. **2013**.

[11] Rosseel, T.M.; Remec, I.; Field, K.G.; Naus, D.J. Evaluating the Effects of Irradiation on Concrete at Extended Lifetimes Light Water Reactor Sustainability Newsletter **2013**.

[12] Kaplan, M.F. *Concrete Radiation Shielding*.; Harlow: Longman Scientific, 1989.

[13] Neutron Sources. **2012**, *2016*.

[14] Kontani, O.; Ichikawa, Y.; Ishizawa, A.; Takizawa, M.; Sato, O. Irradiation Effects on Concrete Structures. In Proc. of International Symposium on the Ageing Management & Maintenance of Nuclear Power Plants; pp. 182.

[15] Hilsdorf, H.K.; Kropp, J.; Koch, H.J. The Effects of Nuclear Radiation on the Mechanicals Properties of Concrete. American Concrete Institute Special Publication SP-55 **1978**, 223-251.

[16] Koťátková, J.; Zatloukal, J.; Reiterman, P.; Patera, J.; Hlaváč, Z.; Brabec, P. The Effect of Elevated Temperatures and Nuclear Radiation on the Properties of Biological Shielding Concrete. Key Engineering Materials **2016**, *677*, 8.

[17] Copeland, L.E.; Kanto, D.L.; Verbeck, G.J. Chemistry of Hydration of Portland Cement. In ; pp. 429-431.

[18] Price, B.T.; Horton, C.C.; Spinney, K.T. *Radiation Shielding*.; Pergamon Press: London, 1957.

[19] Hyde, R.B. Fulfilling Requirements for Materials for Nuclear Power Plants. British Nuclear Energy Society **1964**, *3*, 61-64.

[20] Samarin, A. Use of Concrete as a Biological Shield from Ionising Radiation. Energy and Environmental Engineering **2013**, *1*, 90-97.

[21] Malkapur, S.M.; Satdive, H.; Narasimhan, M.C.; Karkera, N.B.; Goverdhan, P.; Sathian, V. Effect of Mix Parameters and Hydrogen Loading on Neutron Radiation Shielding Characteristics of Latex Modified Concrete Mixes. Progress in Nuclear Energy **2015**, *83*, 8-12.

[22] Fowler, D.W. Polymers in Concrete: A Vision for the 21st Century. Cement and Concrete Composites **1999**, *21*, 449-452.

[23] ČSN EN 206-1: Concrete - Part 1: Specification, Performance, Production and Conformity. **2001**.

[24] Clendenning, T.G.; Kellam, B.; MacInnis, C. Hydrogen Evolution from Ferrophosphorus Aggregate in Portland Cement Concrete. Journal American Concrete Institute **1968**, *65*, 1021-1028.

[25] Kolář, K. Použití Těžkých Betonu Ve Stavebnictví. Speciální betony. **2002**, 2, 11-21.

[26] ASTM C637: Specification for Aggregates for Radiation-Shielding Concrete. **2003**.

[27] ASTM C638 – 14: Standard Descriptive Nomenclature of Constituents of Aggregates for Radiation-Shielding Concrete. **2014**.

[28] ACI Committee 349. Evaluation of Existing Nuclear Safety-Related Concrete Structures. Technical Report ACI 349.3R-02 **2002**.

[29] William, K.; Xi, Y.; Naus, D. A Review of the Effects of Radiation on Microstructure and Properties of Concretes used in Nuclear Power Plants. **2013**.

[30] Piotrowski, T.; Tefelski, D.; Polański, A.; Skubalski, J. Monte Carlo Simulations for Optimization of Neutron Shielding Concrete. cent. eur. j. eng **2012**, *2*, 296-303.

[31] D.B. Tefelski; T. Piotrowski; A. Polański; J. Skubalski; V. Blideanu. Monte-Carlo Aided Design of Neutron Shielding Concretes. Bulletin of the Polish Academy of Sciences: Technical Sciences **2013**, *61*, 161-171.

[32] ASME Boiler and Pressure Vessel Code. ASME boiler and pressure vessel code .

[33] Schneider, U. Behaviour of Concrete at High Temeratures. Deutscher Ausschuss Für Stahlbeton **1982**.

[34] Bakos, G.C. Direct Energy Generation and Energy Conservation in Radiation Shielding Facilities. Annals of Nuclear Energy **2001**, *28*, 513-518.

[35] Thomas, D.R. Temperature and Thermal Stress Distributions in Concrete Primary Shields for Nuclear Reactors. Nuclear Engineering and Design **1965**, *1*, 368-384.

[36] Samarin, A. Causes and Effects to be Considered in a Structural Design. In *Concrete Shrinkage*.; Anonymous .; University of Wollongong, Department of Civil Engineering, 1996.

[37] McDonald, D.; Roper, H.; Samarin, A. Prediction Accuracy of Creep and Shrinkage Models for Australian Concrete. In ; pp. 66-78.

[38] Le Pape, Y.; Giorla, A.; Sanahuja, J. Combined Effects of Temperature and Irradiation on Concrete Damage. Journal of Advanced Concrete Technology **2016**, *14*, 70-86.

[39] Aliabdo, A.A.; Elmoaty, Abd Elmoaty M Abd; Auda, E.M. Re-use of Waste Marble Dust in the Production of Cement and Concrete. Construction and Building Materials **2014**, *50*, 28-41.

[40] Khoury, G.A. Performance of Heated Concrete—Mechanical Properties. Contract NUC/56/3604A with Nuclear Installations Inspectorate **1996**.

[41] Pihlajavaara, S.E. Analysis of the Factors Exerting Effect on Strength and Other Properties of Concrete at Elevated Temperatures. In ; pp. 347-354.

[42] Ohgishi, S.; Miyasaka, S.; Chida, J. Properties of Magnetite and Serpentine Concrete at Elevated Temperatures for Nuclear Reactor Shielding. In ; pp. 1243-1253.

[43] Davis, H.S. N-Reactor Shielding. In ; pp. 1109-1161.

[44] Desov, A.E.; Nekrasov, K.D.; Milovanov, A.F. Cube and Prism Stregth of Concrete at Elevated Temperatures. Concrete for Nuclear Reactors **1972**, 423-434.

[45] Davis, H.S. High-Density Concrete made with Hydrous-Iron Aggregate. **1958**.

[46] Du Bois, F. *Beton Lourds Abase De Mineral De Magnetite De Dielette*.; ‖ Centre d'Etudes Nucleaires de Saclay, Commissariat a l'Energie Atomique: France, 1964.

[47] Komarovskii, A.N. *Desing of Nuclear Power Plants*: Atomizdat, Moscow, 1965; pp. 1965.

[48] Massa, G.; De Stefano, R.; Collepardi, M.; Chatterji, S.; Maniscalco, V. Shielding Concretes for Liquid Sodium Cooled Nuclear Reactors. In ; pp. 151-158.

[49] Crispino, E. Studies on the Technology of Concretes Under Thermal Conditions. In ; pp. 443-479.

[50] Weigler, H.; Fischer, R. Influence of High Temperatures on Strength and Deformations of Concrete. In ; pp. 481-493.

[51] Sakr, K.; EL-Hakim, E. Effect of High Temperature Or Fire on Heavy Weight Concrete Properties. Cement and Concrete Research **2005**, *35*, 590-596.

[52] Jaeger, R.G. *Engineering Compendium on Radiation Shielding*.; Springer: Berlin [u.a.], 1975.

[53] Davis, H.S.; Browne, F.L.; Witter, H.C. Properties of High-Density Concrete made with Iron Aggregate Journal of American Concrete Institute **1956**, *27*, 705-26.

[54] Field, K.G.; Remec, I.; Pape, Y.L. Radiation Effects in Concrete for Nuclear Power Plants – Part I: Quantification of Radiation Exposure and Radiation Effects. Nuclear Engineering and Design **2015**, *282*, 126-143.

[55] UPDATE1: World Nuclear Industry Status as of 1 January 2016: Mind the China Effect. **2016**.

[56] Umeki, Y.; Sawada, S.; Mitsugi, S.; Maenaka, T.; Takiguchi, K. Outline of Guidelines for Maintenance and Management of Structures in Nuclear Facilities. Journal of Advanced Concrete Technology **2016**, *14*, 643-663.

[57] Rosseel, T.M.; Maruyama, I.; Le Pape, Y.; Kontani, O.; Giorla, A.B.; Remec, I.; Wall, J.J.; Sircar, M.; Andrade, C.; Ordonez, M. Review of the Current State of Knowledge on the Effects of Radiation on Concrete. Journal of Advanced Concrete Technology **2016**, *14*, 368-383.

[58] Maruyama, I.; Kontani, O.; Sawada, S.; Satu, O.; Osamu, G.; Takizawa, M. Evaluation of Irradiation Effects on Concrete Structure - Background and Preparation of Neutron Irradiation Test. Proceedings of the ASME 2013 Power Conference **2013**.

[59] Kontani, O.; Ichikawa, Y.; Ishizawa, A.; Takizawa, M.; Sato, O. Irradiation Effects on Concrete Structures. Infrastructure Systems for Nuclear Energy **2014**, 459.

[60] British Standards Institute, 4. Specification for Prestressed Concrete Pressure Vessels for Nuclear Reactors. Technical Report BS 4975:1990. **1990**.

[61] Crispino, E.; Fizzotti, C.; Gasparini, R.; Qualtieri, G.; Montagnini, A.; Rossi. Irradiation Effects on Reactor Structural Materials. Fourth United Nations International Conference on the Peaceful Uses of Atomic Energy **1971**, 22.

[62] Dubrovskii, V.B.; Ibragimov, S.S.; Ladygin, A.Y.; Kulakovskii, M.Y.; Pergamenshchik, B.K. Radiation Stability of Serpentine Concrete. Soviet Atomic Energy **1968**, *25*, 1345-1346.

[63] Elleuch, L.; Dubois, F.; Rappeneau, J. Effects of Neutron Radiation on Special Concretes and their Components. Special Publication of The American Concrete Institute 43 **1972**, 1071-1108.

[64] Granata, S.; Montagnini, A. Studies on Behavior of Concretes Under Irradiation. EBST Concrete for Nuclear Reactors **1971**, *34*, 1163–1172.

[65] Dubois, F.; Mauny, P.; Bernard, A.; Elleuch, M. Nouveaux Types De Betons Calorifuges Pour Reacteurs Nucleaires. Proceedings of the Second Information Meeting on Pre Stress Concrete and Reactor Pressure Vessels and their Thermal Isolation **1969**.

[66] Rockwell, T. Physical Tests of Core Drilling from the ORNL Graphite Reactor Shield. **1948**.

[67] Field, K.G.; Remec, I.; Pape, Y.L. Radiation Effects in Concrete for Nuclear Power Plants – Part I: Quantification of Radiation Exposure and Radiation Effects. Nuclear Engineering and Design **2015**, *282*, 126-143.

[68] Maruyama, I.; Kontani, O.; Sawada, S.; Sato, O.; Igarashi, G.; Takizawa, M. Evaluation of Irradiation Effects on Concrete Structure – Background and Preparation of Neutron Irradiation Test. Proceedings of the ASME 2013 Power Conference POWER2013 **2013**.

[69] Bouniol, P.; Aspart, A. Disappearance of Oxygen in Concrete Under Irradiation: The Role of Peroxides in Radiolysis. Cement and Concrete Research **1998**, *28*, 1669-1681.

[70] Vodák, F.; Vydra, V.; Trtík, K.; Kapičková, O. Effect of Gamma Irradiation on Properties of Hardened Cement Paste. Materials and Structures **2011**, *44*, 101-107.

[71] Kontani, O.; Ichikawa, Y.; Ishizawa, A.; Takizawa., M.; Sato, O. chapter Irradiation Effects on Concrete Structures. In *Infrastructure Systems for Nuclear Energy*.; Anonymous .; John Wiley & Sons Ltd, 2014.

[72] Vodák, F.; Trtík, K.; Sopko, V.; Kapičková, O.; Demo, P. Effect of Γ-Irradiation on Strength of Concrete for Nuclear-Safety Structures. Cement and Concrete Research **2005**, *35*, 1447-1451.

[73] Park, S.; Kwon, S.; Jung, S.H. Analysis Technique for Chloride Penetration in Cracked Concrete using Equivalent Diffusion and Permeation. Construction and Building Materials **2012**, *29*, 183-192.

[74] McDowall, D.C. The Effects of Gamma Radiation on the Creep Properties of Concrete. In .

[75] Wittmann, F. Einfluß Des Feuchtigkeitsgehaltes Auf Das Kriechen Des Zementsteines. Rheologica Acta **1970**, *9*, 282-287.

[76] Seeberger, J.; Hilsdorf, H. Einfluß Von Radioactiver Strahlung Auf Die Festogkeit and Struktur Von Beton. Technical Report NR 2505. Institut für Massivbau and Baustofftechnologie **1982**.

[77] Gray, B.S. Effects of Reactor Radiation on Cements and Concrete. **1972**.

[78] Kelly, B.T.; Brocklehurst, J.E.; Mottershead, D.; McNearney, S.; Davidson, I. Effect of Reactor Radiation on Concrete. 2nd Conference on presstressed concrete reactor pressure vessels , 17-39.

[79] Naus, D.J. The Effect of Elevated Temperature on Concrete Materials and Structures - a Literature Review. **2005**.

[80] Schneider, U.; Diederichs, U.; Ehm, C. Effect of Temperature on Steel and Concrete for PCRV'S. Nuclear Engineering and Design **1982**, *67*, 245-258.

[81] Rappeneau, J.; Lagorio, M.; Gilbert, J.; Piron, P. Irradiation Tests of Concretes. Bulletin of the Association for Information Science and Technology **1966**, *110*, 31–48.

[82] Batten, A. Effect of Irradiation on the Strength of Concrete. Technical Report AERE-R 3332. Atomic Energy Research Establishment **1960**.

[83] Structural Effects of Alkali-Silica Reaction – Structural Effects of Alkali-Silica Reaction– Technical Guidance Appraisal of Existing Structures. Institution of Structural Engineers (ISE), **1992**.

[84] Tsuneki Ichikawa; Hitoshi Koizumi. Possibility of Radiation-Induced Degradation of Concrete by Alkali-Silica Reaction of Aggregates. Journal of Nuclear Science and Technology **2002**, *39*, 880-884.

[85] ICHIKAWA, T.; KIMURA, T. Effect of Nuclear Radiation on Alkali-Silica Reaction of Concrete. Journal of Nuclear Science and Technology **2007**, *44*, 1281-1284.

[86] Kurtis, K.E.; Collins, C.L.; Monteiro, P.J.M. The Surface Chemistry of the Alkali-Silica Reaction: A Critical Evaluation and X-Ray Microscopy. Concrete Science and Engineering **2002**, *4*.

[87] Koťátková, J.; Reiterman., P. Preliminary Study on Design of Biological Shielding Concrete – Selection of Binder. Key Engineering Materials **2017**, *722*, 173-177.

[88] ČSN EN 12390-2 - Testing Hardened Concrete – Part 2: Making and Curing Specimens for Strength Tests. **2009**.

[89] ČSN EN 12390-1 Testing Hardened Concrete – Part 1: Shape, Dimensions and Other Requirements for Specimens and Moulds. **2001**.

[90] ČSN 73 1371: Non-Destructive Testing of Concrete – Method of Ultrasonic Pulse Testing of Concrete.

[91] ČSN EN 73 1372: Non-Destructive Testing of Concrete – Testing of Concrete by Resonance Method on Prisms. **2012**.

[92] ČSN EN 12390-3: Testing of Hardened Concrete – Part 3: Compressive Strength. **2002**.

[93] ČSN EN 12390-5: Testing of Hardened Concrete - Part5: Flexural Strength. **2009**.